Aalto University
School of Chemical
Technology

Henni Auvinen

Electrostatic complexation of DNA nanostructures and biomacromolecules

Master's Programme in Life Science Technologies
Major in Biosystems and Biomaterials Engineering

Master's thesis for the degree of Master of Science in Technology submitted for inspection, Espoo, 28 December, 2016.

Supervisor: Professor Mauri Kostiainen

Advisor: Ph.D, Docent Veikko Linko

Aalto University
School of Chemical Technology
Master's Programme in Life Science Technologies

ABSTRACT OF
MASTER'S THESIS

Author:	Henni Auvinen		
Title:	Electrostatic complexation of DNA nanostructures and biomacromolecules		
Department:	Department of Biotechnology and Chemical Technology		
Professorship:	Polymer technology	**Code:**	Kem-100
Supervisor:	Professor Mauri Kostiainen		
Advisor:	Ph.D, Docent Veikko Linko		
Date:	December 28, 2016	**Pages:**	viii + 61

DNA origami folding technique allows the construction of nanoscale structures with almost any arbitrary shape or pattern. The self-assembly and the addressable surface makes the DNA origami method interesting in engineering novel functional materials and molecular-scale devices. However, the susceptibility to nuclease digestion in physiological conditions and poor transfection rates compromises their use in cellular applications, such as drug delivery vehicles.

The aim of this thesis is to coat DNA origamis to improve their structural integrity and transfection rate. Two separate coating systems were studied, both based on the electrostatic and multivalent interactions between a negatively charged origami and positively charged biomacromolecules. The complexation of DNA origamis with the biomacromolecules was studied with agarose gel electrophoretic mobility shift assay and verified with transmission electron microscopy. The structural integrity of the coated origamis was studied by subjecting the origamis to enzymatic digestion by DNase I endonuclease. Finally, the transfection efficiency was studied using confocal microscopy and quantified with fluorescence-activated cell sorting.

The results revealed successful coating of DNA origamis with the protein-dendron conjugate coating system. Two different proteins were used: bovine serum albumin (BSA) and hydrophobin I (HFBI). The proteins were attached to dendrons that served as the synthetic binding unit that attaches to the origami. BSA-coating conferred protection against nuclease digestion and enhanced the transfection efficiency into HEK293 cells. This work proposes a novel coating strategy that could find applications in sophisticated drug delivery and in other nucleotide-based bionanotechnological devices.

Keywords:	DNA nanotechnology, DNA origami, dendrimer, electrostatic binding, cellular delivery
Language:	English

Aalto-yliopisto
Kemian tekniikan korkeakoulu
Life Science Technologies koulutusohjelma

DIPLOMITYÖN
TIIVISTELMÄ

Tekijä:	Henni Auvinen		
Työn nimi:	DNA-nanorakenteiden ja biomakromolekyylien elektrostaattinen kompleksointi		
Laitos:	Biotekniikan ja kemian tekniikan laitos		
Professuuri:	Polymeeriteknologia	**Professuurikoodi:**	Kem-100
Valvoja:	Professori Mauri Kostiainen		
Ohjaaja:	FT, dosentti Veikko Linko		
Päiväys:	28. joulukuuta 2016	**Sivumäärä:**	viii + 61

DNA-origamien valmistustekniikka mahdollistaa lähes mielivaltaisen muotoisten nanokokoisten rakenteiden valmistuksen. DNA-origamien itsejärjestäytyminen sekä mahdollisuus niiden pinnan funktionalisointiin tekee niistä mielenkiintoisen menetelmän valmistattaessa uusia toiminnallisia materiaaleja sekä molekyylikoon laitteita. Fysiologisissa olosuhteissa DNA-origamit ovat kuitenkin alttiita hajottaville nukleaasientsyymeille. Lisäksi DNA-origamit läpäisevät heikosti solukalvon, mikä vaikeuttaa niiden käyttöä esimerkiksi lääkeainekuljettimina.

Tämän diplomityön tarkoituksena on päällystää DNA-origameja niiden solukalvon läpäisevyyden sekä rakenteellisen kestävyyden parantamiseksi. Työssä tutkittiin kahta eri päällystysmenetelmää, jotka molemmat perustuvat elektrostaattiseen vuorovaikutukseen negatiivisen origamin sekä positiivisten biomakromolekyylien välillä. DNA-origamien ja biomakromolekyylien sitoutumista tutkittiin agaroosigeelielektroforeesilla sekä läpäisyelektronimikroskopialla. Rakenteellista stabiilisuutta tutkittiin altistamalla päällystetyt DNA-origamit DNase I -endonukleaasin hajottamiselle. Lopuksi päällystettyjen origamien soluläpäisevyyttä HEK293-soluihin tutkittiin konfokaalimikroskopialla sekä kvantitatiivisesti FACScan-virtaussytometrialla.

Tulokset osoittivat DNA-origamien päällystämisen onnistuvan proteiini–dendroni -konjugaatteihin perustuvalla päällystysmenetelmällä. Konjugaatissa dendronit muodostivat synteettisen DNA:han sitoutuvan osan, johon voitiin edelleen kiinnittää proteiineja. Kaksi käytettyä proteiinia olivat naudan seerumialbumiini (BSA) sekä hydrofobiini I (HFBI). Näistä BSA-päällystyksen todettiin suojelevan origameja nukleaasien hajottamiselta sekä parantavan origamien soluläpäisevyyttä HEK293-soluihin. Tämä työ esittelee uuden DNA-origamien päällystysmenetelmän, jota voitaisiin hyödyntää lääkeainekuljetussovelluksissa sekä muissa nukleotidirakenteisissa bionanoteknologian sovelluksissa.

Asiasanat:	DNA nanoteknologia, DNA origami, dendrimeeri, elektrostaattinen sitoutuminen, solukuljetus
Kieli:	Englanti

Acknowledgements

This thesis was conducted in the Biohybrid Materials group at Aalto University in the School of Chemical Engineering. This thesis project was extremely interesting and rewarding, and most importantly, I learned a lot!

First of all, I want to thank professor Mauri Kostiainen for the opportunity to join his research group and learn about the academic world. The greatest gratitude goes to my advisor Veikko Linko, who has guided me into the field of DNA nanotechnology. I would also like to thank Joona Mikkilä and Sami Nummelin for providing the Janus dendrimers, and Hongbo Zhong and Hélder Santos for performing the cell culture studies at the University of Helsinki in the Faculty of Pharmacy. In addition, I want to thank all the incredible members of the Biohybrid Materials group and especially Sanna who has been my peer support during this thesis.

I also want to thank my family and friends for supporting me during all these years. Great gratitude goes also to my dear friend Erika, who has been with me since the first day of university. Last but not least, I want to thank Mika who has helped me probably with all the courses at the uni.

Espoo, December 28, 2016

Henni Auvinen

Abbreviations and Acronyms

2D	Two dimensional
3D	Three dimensional
60HB	60-helix bundle
AFM	Atomic force microscopy
aPCR	Asymmetric polymerase chain reaction
AuNPs	Gold nanoparticles
BG	Benzylguanine
BSA	Bovine serum albumin
CCMV	Cowpea chlorotic mottle virus
CH	Chlorohexane
CP	Capsid protein
CpG	Cytosine-phosphate-guanine
DAPI	4',6-diamidino-2-phenylindole
DNA	Deoxyribonucleic acid
DNase I	Deoxyribonuclease I
Dox	Doxorubicin
dsDNA	Double-stranded DNA
DX	Double-crossover
EDTA	Ethylenediaminetetraacetic acid
EMSA	Electrophoretic mobility shift assay
EthBr	Ethidium bromide
FACS	Fluorescence-activated cell sorting
FBS	Fetal bovine serum
GOx	Glucose oxidase
hAGT	O6-alkyltransferase
HEK293	Human embryonic kidney 293
HFBI	Hydrophobin I
HRP	Horseradish peroxidase
IgG	Immunoglobulin G
$MgCl_2$	Magnesium chloride

mRNA	Messenger RNA
MTT	Methylthiazol tetrazolium
NaCl	Sodiumchloride
NTA	Ni-nitriloacetic acid
PCR	Polymerase chain reaction
PEG	Polyethylene glycol
RNA	Ribonucleic acid
RNAi	RNA interference
siRNA	Small interfering RNA
ssDNA	Single-stranded DNA
TEM	Transmission electron microscopy
TLR9	Toll-like receptor 9
Tris	Tris(hydroxymethyl)aminomethane
TX	Triple-crossover

Contents

Chapter 1

Introduction

The field of structural DNA nanotechnology has grown rapidly during the last two decades, as it allows the construction of novel functional materials and molecular-scale devices from nucleic acids. Structural DNA nanotechnology was established by Ned Seeman in the 1980s [1], who constructed various DNA motifs that could be used to self-assemble DNA nanostructures. The idea that DNA could be used as a construction material was revolutionary, as DNA was previously only considered as a genetic material.

Structural DNA nanotechnology is based on the self-assembly of single-stranded DNA into double-helical DNA by complementary base pairing. One of the most used methods in DNA nanotechnology is the DNA origami folding technique introduced by Paul Rothemund in 2006 [3], where a long single-stranded DNA is folded into desired shapes with the help of numerous short complementary single-strands of DNA. The self-assembly of nanoscale structures and the addressable surface, which allows the selective functionalization of biomolecules and nanomaterials, makes the DNA origami method extremely interesting in engineering novel functional materials and molecular-scale devices.

During recent years, DNA origamis have been studied as drug delivery carriers for molecular medicine as they are inherently biocompatible and the structure may include cell-specific ligands and spatially organized drug molecules. However, instability in physiological conditions, innate immune activation and poor transfection rates compromise their use in *in vivo* applications. Cells and organisms have complex mechanisms to detect and degrade foreign DNA from invading pathogens [4]. Thus, one of the biggest challenges also for synthetic nucleotide-based construct materials is to escape and survive from this natural defense mechanism. A protective coating over the origami could provide a novel approach to yield DNA origamis with improved structural and transfection properties benefiting drug delivery and

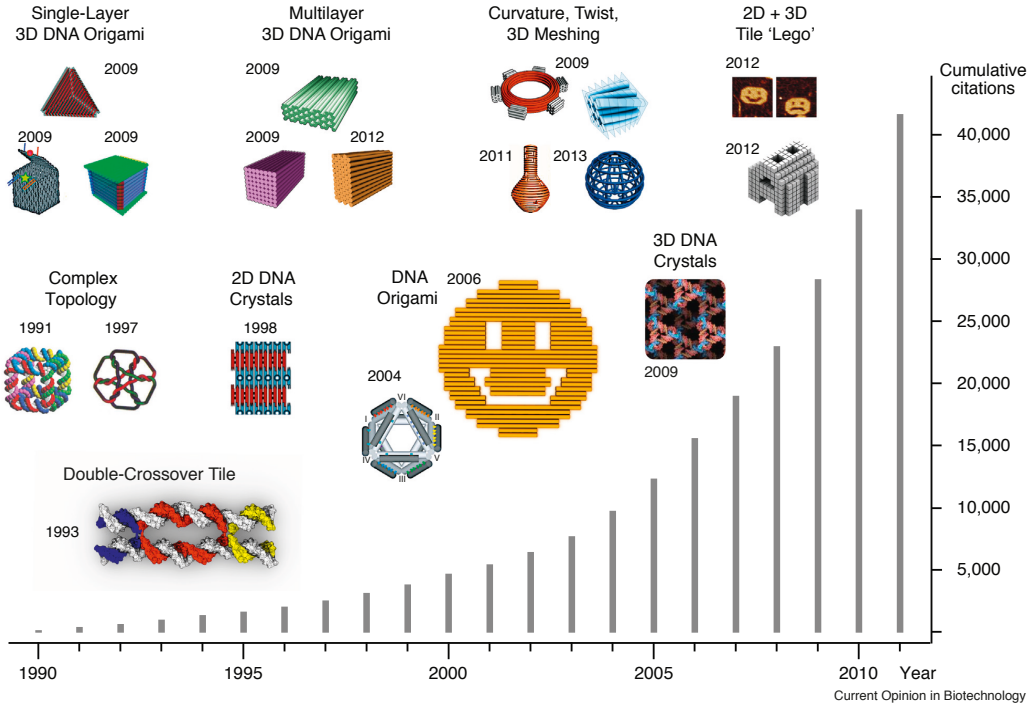

Figure 1.1: Timeline illustrating the evolution of structural DNA nanotechnology and the increasing interest towards the field. The lower panel histogram depicts cumulative citations to the selected set of articles. [2]

other nucleotide-based bionanotechnological devices.

This thesis establishes a novel and highly modifiable coating strategy based on electrostatic interactions to enhance the structural integrity and the cellular uptake of DNA origamis. Chapter 2 reviews the basic structure and properties of DNA and introduces simple DNA nanostructures. In Chapter 3, the DNA origami method is discussed and some of its applications are introduced. This chapter also discusses biocompatibility and stability of DNA nanostructures. Chapter 4 introduces dendrimers and dendrons and provides an overview of the central binding phenomena essential in the complexation of DNA origamis and dendrimers. The materials and methods of the research are presented in Chapter 5 and the results in Chapter 6.

Chapter 2

DNA

At the beginning of the 1950s, the three-dimensional structure of deoxyribonucleic acid (DNA) was analyzed with X-ray diffraction technique. This analysis confirmed DNA to be a rather simple polymer consisting of two strands wound into each other, forming a helix. The complete structure of DNA was revealed in 1953, when the Watson–Crick model was introduced. [5]

Until the last two or three decades, DNA was regarded only as the genetic material that carries the instructions for growth, development, functioning and reproduction of an organism. Today, DNA has been recognized to be an attractive construction material due to its nanoscale controllability, biocompatibility, biodegradability and its molecular recognition capacity. Different kinds of nanostructures, such as ordered lattices, origami and supramolecular assemblies have been constructed. [6] In this chapter, the structure and properties of DNA are discussed.

2.1 Structure of DNA

DNA is a linear polymer composed of two complementary polynucleotide chains coiled around each other. Nucleotides form the polynucleotide chain and are composed of three characteristic components: a five-carbon ring sugar called deoxyribose, a phosphate group and a nitrogen-containing base. The phosphate group of the nucleotide is attached to the 5' carbon of the deoxyribose, whereas the base is attached to the 1' carbon. The nitrogenous bases are heterocyclic aromatic ring systems that belong either to monocyclic pyrimidines or to bicyclic purines. DNA contains two purine bases, adenine (A) and guanine (G), which have fused five and six atom rings, and two pyrimidines, cytosine (C) and thymine (T), which are composed of a single six-membered

ring. The nucleotides are covalently linked by phosphodiester bonds, where 5'-phosphate group of one nucleotide is joined to the 3'-hydroxyl group of the next nucleotide's sugar, resulting in alternating sugar-phosphate backbone, as illustrated in Figure 2.1. [7]

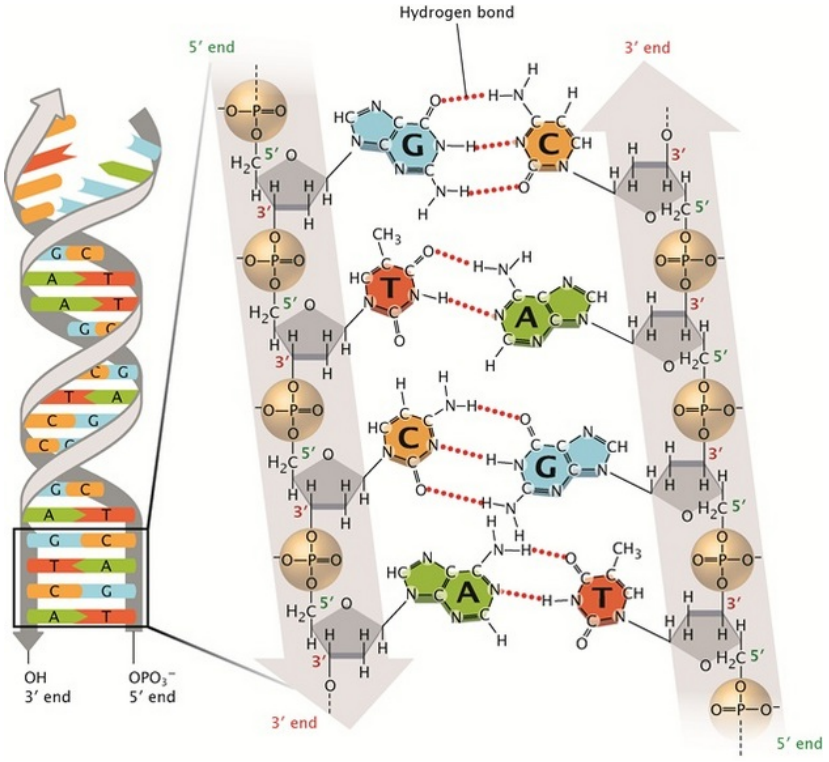

Figure 2.1: Structure of DNA. The DNA double helix is formed according to the Watson–Crick model: C and G, and A and T forms hydrogen bonds. Sugar-phosphate backbones run antiparallel to each other. [8]

The polynucleotide chains in the double helical structure are held together by hydrogen bonds between the purines and pyrimidines according to hydrogen-bonding patterns in the Watson–Crick model: adenosine can only pair with thymine and guanine with cytosine. In order to facilitate the complementary base pairing, the strands need to be antiparallel to each other and thus have different polarity. The 5' end of one strand is adjacent to the 3' end of the other strand, as can be seen in Figure 2.1. The base pairs are packed inside the DNA helix, thus leaving the sugar-phosphate backbone on the outside and giving a negative charge for DNA at pH 7. Moreover, to pack the base pairs efficiently, the sugar-phosphate backbones are twisted around a common axis to form a right-handed double helix. In a most common DNA

conformation (B-DNA), a complete turn is formed after 10.5 base pairs and the double-helix raises 36 ångströms (Å) per turn. [5, 7, 9]

In base pairing, adenine and thymine will form two hydrogen bonds with each other, whereas cytosine and guanine will form three. Therefore, the energetic stabilization in the vacuum that results from the hydrogen bond formation for G–C is 46 kJ/mol, which is higher than 25 kJ/mol for the A–T base pair. Thus, the more C–G pairs a DNA double helix includes, the more stable it is. Although hydrogen bonding between bases is important during the formation of DNA double helices, they do not contribute to the overall stability as much as the base stacking interactions. The bases in DNA contain specially polarized aromatic ring systems that distribute polarization around the ring. Individual atoms have partial charges that are not symmetrically distributed. As the bases stack on top of each other in the helical DNA, the partial charges will overlap so that the negative charges will be close to the positively charged ones, thus stabilizing the structure. In addition, the bases are planar in structure, which allows them to stack well on top of each other. [9]

DNA double helices can form several different conformations depending on the surrounding environment. The most typical conformations are A-, B- and Z-DNA, of which B-DNA is the 'standard' conformation of DNA – originally described by Watson and Crick. These three conformations for DNA are illustrated in Figure 2.2. B-DNA is the most stable structure under physiological conditions. It has its base pairs nearly perpendicular to the axis of the helix and located right in the center of the axis. In B-DNA, the ribose ring has its sugar pucker in C2' endo conformation. One helical turn is formed with 10.5 base pairs, which equals 3.4 Å helix rise per base pair. A-DNA is common in solutions devoid of water. It forms a right-handed double helix just like B-DNA, but its base pairs are displaced off-axis towards the minor groove making the plane of the base pairs tilted with respect to the helix axis. The C3' atom is in endo conformation and one turn takes approximately 11 base pairs, which equals 2.6 Å helix rise per base pair. Therefore, the major groove is much narrower than in B-DNA, whereas the minor groove is wider. In addition to the right-handed A- and B-forms, a left-handed form of DNA, Z-DNA, was discovered by Alexander Rich in 1979. Z-DNA is formed mostly by alternating C and G nucleotides, but some substitutions of A with G and T with C may occur. The sugars alternate from 2' endo to 3' endo puckers in Z-DNA. One helical turn is formed with 12 base pairs, which equals 3.7 Å helix rise per base pair. [7, 10]

DNA hybridization refers to the annealing of two complementary single strands into a double strand. On the contrary, due to the relative weakness of hydrogen bond strength between the base pairs, DNA double strands can

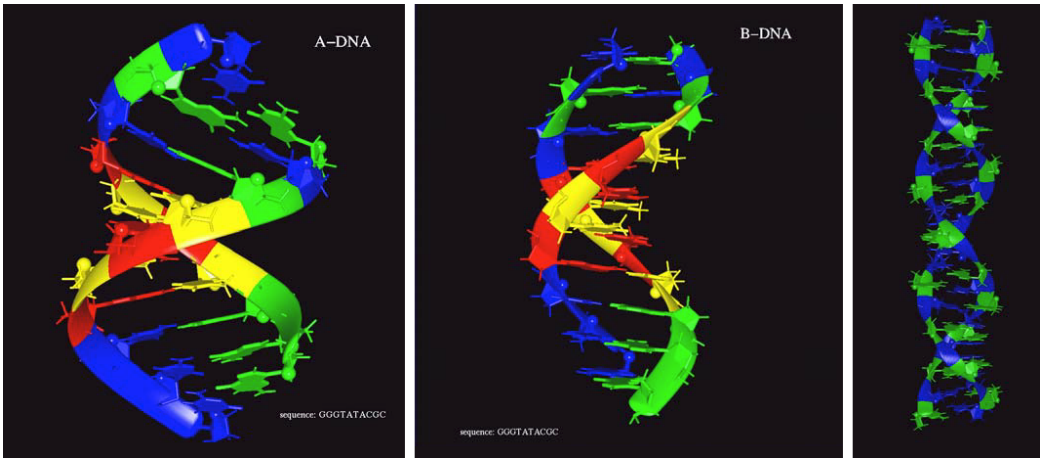

Figure 2.2: Models of A-, B- and Z-DNA conformations. B-DNA is the standard conformation of DNA, A-DNA is tilted respected to the axis, and Z-DNA forms a left-handed helix. [11]

be denatured into two single strands by exposure to heat, or by changing pH or salt concentration. The melting temperature of duplex DNA thus depends on the base composition, length of the strand and the salt concentration. [10]

2.2 Simple DNA constructs

DNA has many properties, such as accurate molecular recognition, nanoscale dimensions, programmability through self-assembly and biocompatibility that makes it an excellent choice for nanometer-level fabrication. Structural DNA nanotechnology aims to use DNA motifs to build two- and three-dimensional target shapes and structures, where different motifs are combined by sticky-ended cohesion, edge sharing or paranemic interactions of double helices. Sticky-ended cohesion, where DNA double helices with complementary single-stranded overhangs connect by base-pairing, and ligation have been used for many years to construct linear DNA molecules for genetic engineering. However, linear DNA motifs cannot yield more complicated nanostructures in two or three dimensions. The self-assembly of structurally more complex DNA constructs is based on combining complementary sticky-ended cohesion with branched DNA motifs, which therefore allows the bottom-up construction of nanoscale objects. [12]

The idea to build nanoshapes using DNA molecules was introduced by Nadrian 'Ned' Seeman in the 1980s [13]. Seeman proposed an unsymmetrical

four-armed branched DNA molecule (Figure 2.3A) that is based on the Holliday junction (found in nature in a genetic recombination process). These branched constructs are composed of four oligonucleotides and can be attached to similar constructs with sticky-ends to yield more complex two-dimensional (2D) lattices. These lattices are, however, rather flexible, and thus Seeman and his coworkers constructed more robust structures called crossover tiles. Double-crossover (DX) tiles (Figure 2.3B) are composed of two DNA double helices that are joined together with two Holliday junctions, whereas triple-crossover (TX) tiles are formed of three double helices. Crossover tiles can be used to produce different 2D and three-dimensional (3D) shapes and structures. [6] Unfortunately, there are certain disadvantages to the tile-based assembly of DNA nanostructures. The method requires exact stoichiometric control of oligonucleotides, which may result in low yields due to experimental errors. Moreover, the method is limited to basic geometric structures and the repeating building blocks makes it difficult to create spatially addressable objects. [14]. A revolutionary breakthrough occurred in 2006, when Paul Rothemund introduced the DNA origami folding technique, which allows fabrication of almost any arbitrary nanoscale pattern and shape [3]. DNA origamis will be discussed in more detail in Chapter 3.

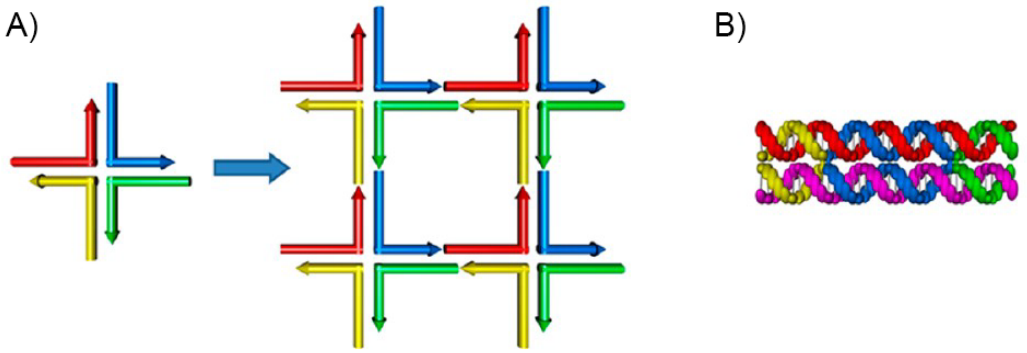

Figure 2.3: A) Unsymmetrical four-armed branched DNA motifs can be combined with sticky-ends to yield two-dimensional (2D) structures. B) Double-crossover tile. Adapted from [15].

Chapter 3

DNA origami

The tile based method introduced in Section 2.2 is a promising method of constructing small and simple geometric shapes with repeating DNA building blocks. However, the DNA origami method provides a useful tool for building more sophisticated structures with almost any arbitrary nanoscale pattern or shape with molecular weights in the megadalton regime. The DNA origami method was first introduced by Paul Rothemund in 2006 [3], and it is based on folding a long single-stranded DNA into target structures. The term 'origami' refers to the Japanese art of folding paper, whereas in the DNA origami method, the long single-stranded DNA called 'scaffold' is folded into desired shapes with the help of numerous short complementary single-strands of DNA – called 'staple strands' (Figure 3.1). This folding technique enables the construction of highly addressable 2D and 3D DNA nanostructures with (sub)nanometer-scale resolution. The self-assembly and the addressable surface, which allows the selective functionalization of biomolecules and nanomaterials, makes the DNA origami method extremely interesting and opens up possibilities to several applications. Moreover, the DNA origami method is robust, fast and defect-free method without the need for stoichiometric studies or strict control over the quality and quantity of the staple strands. [14]

3.1 Preparation of DNA origamis

The viral genomic DNA isolated from M13mp18 phage is commonly used as the long single-stranded scaffold in the DNA origami method. This circular genome is 7249 nucleotides long and forms roughly an area of 8500 nm^2 when fully base-paired with staple strands (assuming a 1.5 nm gap between the adjacent helices). In general, the length of the scaffold strand determines

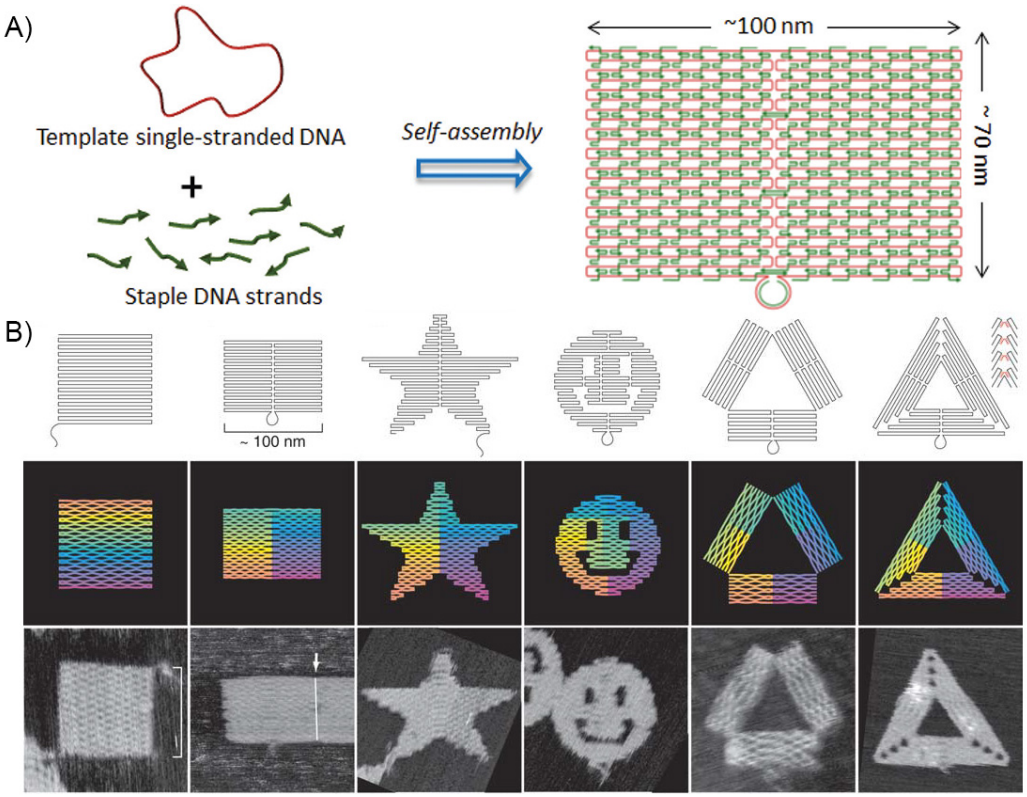

Figure 3.1: DNA origami method. A) A long single stranded DNA is folded into the desired shape with numerous staple strands. Adapted from [16] B) Design and AFM pictures of DNA origami shapes. Adapted from [3]

.

the size of the structure. As a result, alternative scaffolds have been created in order to create origami structures that are not restricted by the size of the M13mp18 scaffold. [17] Polymerase chain reaction (PCR) [18] or asymmetric PCR (aPCR) [19] can be used to create arbitrary sized single-stranded scaffolds. In standard PCR, the products can be separated by using biotinylated 3' primers, which allow the biotinylated PCR products to bind to streptavidin-coated magnetic beams. In the DNA origami method, single-stranded scaffolds are commonly used to avoid the competing reannealing of the complementary strands with double stranded scaffolds. However, Högberg *et al.* [20] have proved that double-stranded DNA can be used in a one-pot reaction to form two discrete structures. This can be carried out by using annealing protocols with a fast temperature drop and by removing the forming formamide, which is a denaturant in the reaction. Moreover, scaffold-free

methods have been reported, where short single-stranded DNA (ssDNA) components called 'DNA bricks' are used to create desired structures [21].

Staple strands are synthetically produced short DNA strands, usually ranging from 16 to 60 nucleotides in length. They bind complementary to the scaffold DNA, which drives the formation of the desired structure. Staple strands connect neighboring adjacent helices and hold the structure together, as seen in Figure 3.2. Dozens of staple strands are needed to fold the whole single-stranded M13 phage genome. [17] The relative stoichiometric ratio of the staple strands is not critical, as the staple strands hybridize more readily with the common scaffold than with each other. Moreover, possible errors in the folding, such as misplaced or truncated sequences, are displaced by strand invasion and other exchange mechanisms. [14]

DNA origamis are folded in a one-pot reaction by mixing the single-stranded scaffold strand with the excess of staple strands in a specific buffer. Typically (as in this thesis) the buffer contains Tris(hydroxymethyl)aminomethane, ethylenediaminetetraacetic acid (EDTA), acetic acid and Mg^{2+} ions. The buffer provides suitable pH for DNA ($\sim$8), and the role of Mg^{2+} ions is to stabilize the origami structure by neutralizing adjacent phosphodiesters at the crossovers by preventing negative charge-repulsion. [17] However, magnesium ions may cause DNA degradation and unwanted enzymatic activity. Martin and Dietz [22] showed that multilayer origamis can also be folded in the presence of monovalent sodium ions instead of multivalent ions, such as magnesium. The concentration of the sodium ions, however, may need to be even 100 times higher than the magnesium ion concentration for full assembly of an origami structure. The folding mixture is exposed to a thermal annealing process where the solution is first heated to 60–90 °C to denaturate any pre-existing secondary structures, followed by slow cooling. As the solution cools down, the staple strands bind to the scaffold DNA according to the Watson–Crick base-pairing and pull the scaffold strand into the desired shape forming closely packed B-DNA bundles. [23] In addition to thermal gradient based assembly, DNA origamis can also be assembled at constant temperatures, either by slowly decreasing the concentration of a denaturant [24] or by using structurally designed single-stranded tiles that can be tuned to assemble isothermally across a wide range of temperatures [25]. DNA origamis can be purified from excess staple strands by using agarose-gel extraction, rate-zonal centrifugation [26], spin-filtering [27] or poly(ethylene glycol) (PEG) precipitation method [28]. The desired structure can be confirmed with atomic force microscopy (AFM) and negative-stain or cryogenic transmission electron microscopy (TEM).

3.2 Principles of DNA origami design

The first step in designing a DNA origami is to raster-fill the desired structure with the single-stranded scaffold DNA so that it comprises one of the two strands in every helix, as seen in Figure 3.2. The scaffold sequence serves as an input to design the sequences of the staple strands – staples are unique in sequence and bind complementary to the scaffold according to the Watson-Crick base pairing. The double-helical domains are connected to each other by interhelical bridges, such as immobilized Holliday junctions. These connections are usually antiparallel crossovers formed by staple or the scaffold strands between adjacent double helical domains. However, it is more common that the staple strands form most of the crossovers, and they can also form multiple crossovers between double helical domains. The position of the crossovers depends on the packing lattice rules of the desired structure. [23] In addition, single-stranded domains can be included in the structure, for instance, to provide entropic springs [29] or to prevent unwanted base-stacking between object interfaces as straight ends on the edge of origamis tend to stick together due to hydrophobicity [3]. Blunt-ended base-stacking interactions can, however, also be used to construct multidomain assemblies from shape-complementary components [30].

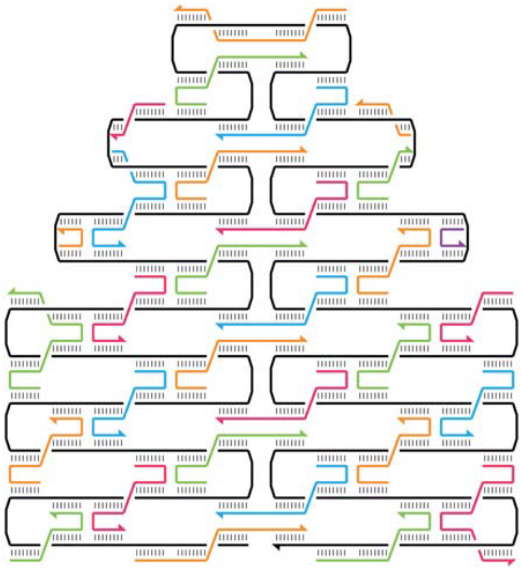

Figure 3.2: The scaffold strand (black) runs through the whole structure back and forth, and the staple strands bind complementary to multiple parts in the scaffold holding the structure together [17].

3.2.1 2D DNA origami

In the original work by Rothemund, different planar 2D structures, such as rectangular shapes, stars, smiley faces and triangles were prepared. In this approach 2D origami structures are prepared by following a design principle, in which adjacent helices are connected by crossovers interspaced by 1.5 helical turn, which equals 16 base pairs for B-DNA. This design principle creates interhelical connections every $\sim 180°$, which are needed for 2D structures. [3] Single-layer origami structures can be assembled with nearly 100 % yield in just a few minutes [31].

One major challenge in the DNA origami development is to scale up the size of the DNA origami structures. Larger structures can be created by simply connecting individual origami tiles with sticky-ended or blunt-end cohesion. Another interesting method to scale up DNA origami is to use DNA tiles as folding staples instead of short oligonucleotides to fold the M13 scaffold. It is even possible to use DNA origamis to fold a scaffold strand, thus reaching the size of micrometer scale. [32]

3.2.2 3D DNA origami

One of the major drawbacks of two-dimensional origami structures is their weak resistance to mechanical stress. For this reason, various kinds of 3D origami structures have been created to yield more rigid structures. 3D origami structures can be prepared with two different strategies. In the first method, 3D origami structures are prepared from 2D origami sheets, which are connected with additional strands between interfacing helices at the edges. This approach can be used to create structures with internal cavities, such as closed polyhedras and prismlike structures. DNA origamis are stable enough to be heated up to 50 °C for secondary annealing. [16]

In the second method, crossovers are arranged in a defined way to position adjacent antiparallel double-stranded DNA (dsDNA) to yield tubular or multilayered structures. The positioning of the crossovers depends on the packaging lattice and thus determines how adjacent helices are connected. [16] In the regular multilayered origami, each double helical domain has up to three neighboring helices arranged in a three-fold symmetry. The resulting structure has a hexagonal cross-section, which resembles of a honeycomb lattice. The crossovers are spaced by using 7 bp segments, so that the crossover interval between a particular pair of neighboring helices is 21 bp (2 times full helical turn of dsDNA). In addition, twisting and bending can be introduced into the structure by deleting or inserting nucleotides in the segments of the adjacent helices. The similar design rules can be used to prepare DNA objects

in square lattice packaging, where double-helical domains are arranged in a fourfold symmetry so that each double helix in the structure has up to four neighboring helices. To create square lattices, segments are placed in intervals of 8 bp so that the crossover interval between a particular helix pair is 32 bp (close to 3 full helical turns of dsDNA). However, this spacing rule causes underwining as the helicity of double helical domains in B-DNA differs from the native 10.5 bp per turn to the imposed 10.67 bp. This causes global twisting for the entire structure, which can be eliminated by varying the spacing between the crossovers. [23] Different crossover patterns to create 2D and 3D structures are illustrated in Figure 3.3. Commonly, the folding of 3D origami structures requires longer folding times than for 2D objects [16].

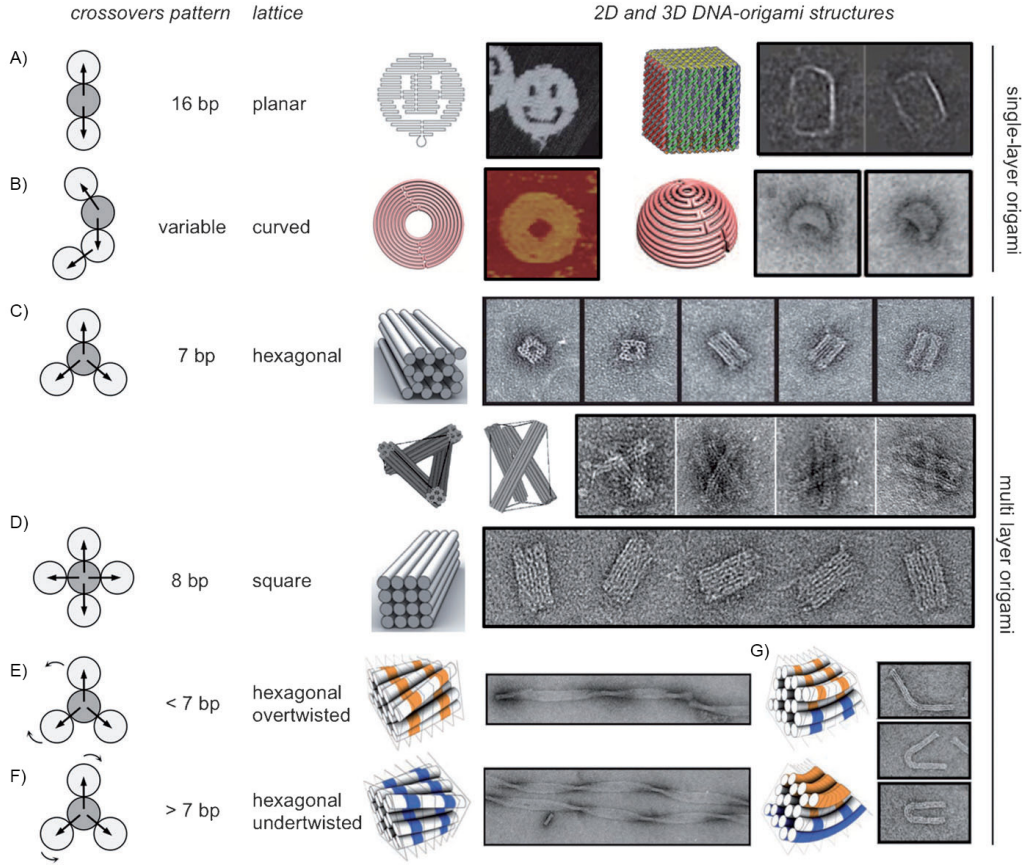

Figure 3.3: Different crossover patterns and the corresponding structures. Single-layer (A, B) and multilayer (C–G) structures with curvature and twisting can be designed with suitable crossover-patterns. Adapted from [14].

3.2.3 Computational tools for DNA origami

DNA origamis can be designed by using several computational tools. An open-source DNA origami design software caDNAno is commonly used to design the strand routing and the sequences of DNA strands, whereas CanDo software can be used to determine the solution shape and mechanical fluctuations of the structure. These software, however, require manual intervention – the user needs to sketch a blueprint of the structure and define the DNA sequences, which requires basic knowledge of structural properties and possible folding pathways. [33]

Only recently, new design approaches have been introduced to replace these bottom-up designs. Benson *et al.* [34] introduced the first top-down design software called vHelix for DNA origami design. Instead of close-packed helices, this software is based on creating a polyhedral meshwork of the target structure and then using a routing algorithm to route the scaffold through the meshed structure. However, this semi-automated approach is based on single duplex edges, which may result in unstable structures. Moreover, it limits the designed structures to spherical topologies. Thus, Veneziano *et al.* [19] introduced a fully automated procedure called DAEDALUS (DNA origami sequence design algorithm for user-defined structures) that allows designing almost any origami structure based only on its target shape. The objects are presented as meshed origami structures, which allows a spanning tree algorithm to route the linear scaffold strand through the target shape and to design the staple strands with minimal human input. This approach uses wireframe motifs in which inter-connected edges consist of two double stranded DNA helices that are joined using antiparallel double crossovers (DX).

3.3 Applications

The self-assembly of nanoscale structures and the highly addressable surface, which allows the selective functionalization of biomolecules and nanomaterials, makes the DNA origami method extremely interesting in a wide range of applications, including single molecular recognition and analysis [35], functional nanomechanical molecular devices [36, 37], nanoelectronics [38] and cellular applications [16]. DNA origami nanostructures have particularly great potential in biological applications, for example in drug delivery and in living-cell analysis. The structures are inherently biocompatible, they show slight resistance against several endo- and exonucleases, and they are compatible with functional biomolecules, such as proteins and aptamers. [4, 16]

3.3.1 Material organization

One of the most significant features of DNA origamis is their highly addressable surface that allows selective functionalization of the structure as each individual position in the origami is defined by its unique sequence information. This property makes DNA origamis promising platforms for the specific arraying of wide range of materials, such as proteins [39] and inorganic nanomaterials [38, 40]. Decoration of DNA origamis with functional moieties is important for the wide range of applications as DNA molecules have limited chemical, optical and electronic functionalities [14].

DNA origamis can be used for the site-specific patterning of protein molecules, which allows researchers to study protein-protein interactions and to construct novel biomaterials for applications such as tissue engineering [41]. The critical issue in protein immobilization on DNA origami is how to bind a staple strand to the target protein. One way to link proteins with DNA origamis is to use nickel-mediated interaction between a hexahistidine (His_6)-tag added to the end of a protein's backbone, and origami functionalized with Ni-nitriloacetic acid (NTA). This site-specific linkage can be controllably broken by addition of excess imidazole that binds nickel. [42] In another study, Kuzyk *et al.* [39] demonstrated that 5' biotin-modification of specific staple strands allowed streptavidin binding at specific locations on the origami (Figure 3.4A). Linko *et al.* [43] used biotin-avidin-biotin linkage to attach glucose oxidase (GOx) and horseradish peroxidase (HRP) inside different origami units. They demonstrated that the seperate units could be combined resulting in a nanoreactor that is capable of performing enzyme cascade reactions. Proteins can also be coupled on DNA origamis with reversible antibody-antigen interactions, aptamer binding, and through nucleic acid hybridization of DNA tagged proteins [44]. Moreover, sequence-selective recognition molecules could be used to attach functional molecules and particles on DNA origamis [16]. Zinc finger proteins can recognize specific sequences in DNA. Each domain in the protein can recognize three base pairs, and by designing new proteins by combining these domains; longer DNA sequences can be specifically recognized. Binding sequences can be added to these proteins to allow specific binding of target proteins. [45]

Besides proteins, DNA origamis are promising platforms for the organization of inorganic nanomaterials, such as metal nanoparticles [40, 46, 47] and carbon nanotubes [38]. Inorganic nanomaterials are commonly arrayed on origamis through complementary strand hybridization, where the particles are DNA-tagged with sequences that can hybridize with the terminal extensions of staple strands in the origami structure [14]. Triangular-shaped origamis have been used to organize gold [40] (Figure 3.4B) and silver [46] nanoparticles

through DNA hybridization at predesigned positions. The gold and silver nanoparticles were functionalized with thiolated ssDNA strands, which can further bind to complementary staple strand sequences on the origami surface. These kind of hybrid materials where origamis are arrayed with metal nanoparticles, could be used to study the photonic and distance-dependent effect of plasmonic coupling of metal nanoparticles, with promising applications in sensing and optical devices [14]. For instance, Kuzyk *et al.* [47] arranged gold nanoparticles on DNA origami bundle to create plasmonic devices with optical activity. Moreover, carbon nanotube-origami hybrids for the possible use in nanoelectronics have been described recently. Maune *et al.* [38] positioned two DNA-modified carbon nanotubes on DNA origamis through hybridization (Figure 3.4C). The nanotubes were aligned into cross-junctions in a way that showed field-effect transistor-like behavior.

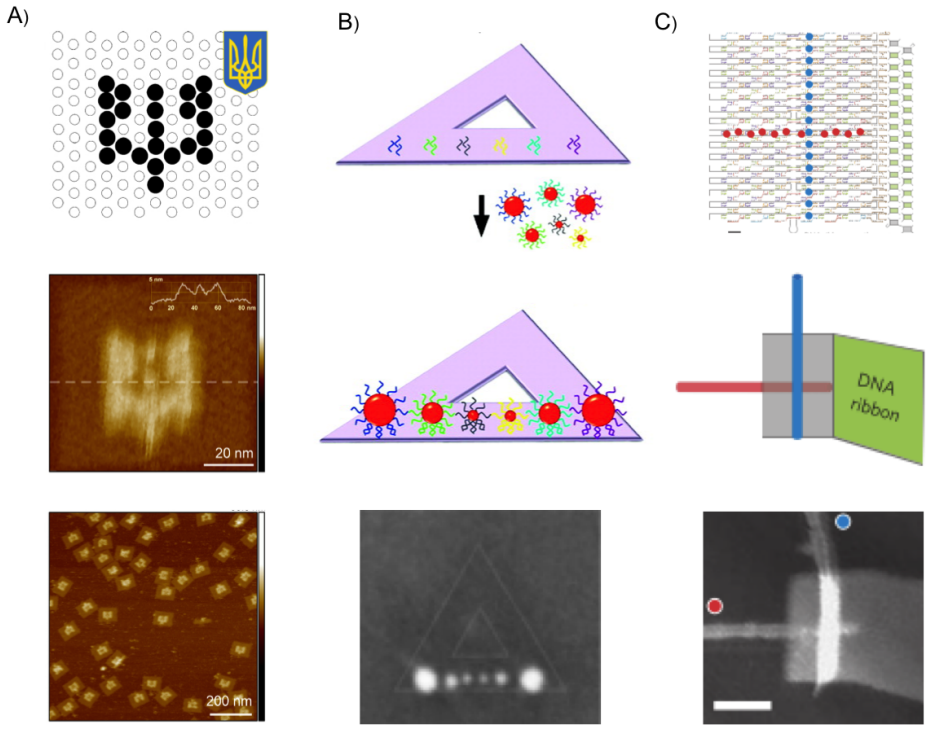

Figure 3.4: A) Biotin modificated origami allowed streptavin binding to specific locations to resemble the coat of arms of Ukraine. Imaged by AFM. Adapted from [39] B) Gold nanoparticles organized at predesigned positions by a triangular-shaped origami. Imaged by SEM. Adapted from [40]. C) Carbon nanotubes positioned into cross-junctions on a DNA origami. Imaged by AFM. Adapted from [38].

3.3.2 Single molecular recognition and analysis

DNA origamis can be used for single-molecular analysis of chemical and biochemical processes. Single-molecular events are complex to study in a bulk approach as many molecules contribute to the measured signal. However, all biochemical reactions are actions of single enzymes, nucleic acids or proteins, and thus single-molecular analysis is important for understanding chemical and biochemical reactions. As different functionalities can be placed on the origami surface, DNA origamis can act as probes for molecular recognition to isolate single molecules for unimolecular investigations. [35]

One of the first examples of single-molecular analysis using DNA origamis was reported by Ke *et al.* [48] in 2008 where nucleic-acid probe tiles were used to detect label-free ribonucleic acid (RNA) hybridization. These 20-nucleotide-long single-stranded DNA probes placed on an origami can selectively bind to their RNA targets in solution. After binding, the DNA-RNA hybrids are adsorbed on mica and easily detected by AFM. This promising method could be used to detect low levels of gene expression, possibly even at a single-cell level. [48] DNA origami based single-molecular analysis is also used for studying conformation changes in DNA, such as the formation of G-quadruplexes. G-quadruplexes inhibit telomerase activity and are thus promising anticancer targets [49]. In a recent work, DNA origamis were used to detect single-nucleotide changes in DNA-code that might indicate propensity to, or protection from certain diseases [50]. Moreover, Voigt *et al.* [51] demonstrated that DNA origamis can be used for analyzing single-molecule chemical reactions. Individual bond cleavage and formation reactions were achieved and visualized on the origami surface via biotin-streptavidin complexes. The formation and cleavage reactions led to either binding or removal of the complexes from the origami surface. This method could be used to study chemical processes and also to produce macromolecules in a highly selective way compared with traditional synthesis.

3.3.3 Drug-delivery systems

DNA origamis are well-suited for drug-delivery carriers due to their excellent and modular properties, such as predictable and well-defined structure, structural stability, biocompatibility and ability to be internalized by cells. Several methods can be used to couple DNA with functional cargo molecules, including covalent modification, hybridization, avidin-biotin interactions, intercalation in DNA duplex and encapsulation into box-like origamis. Moreover, the addressable surface allows precisely control the position of the cargo molecules, which is impossible with organic and inorganic nanomaterials. Different

cargos, including nucleic acids, proteins, such as vaccines and immunoglobins, and several small molecules could be coupled to DNA origamis. [52]

The inherent compatibility between the cargo and the carrier makes the loading procedure easy for nucleic acid -based cargo as they can be simply hybridized or integrated into the structural sequence. siRNAs is part of the biological RNA interference (RNAi) process in which it inhibits gene expression by binding and degrading complementary messenger RNAs (mRNA), thereby suppressing the expression of a target protein. [52] Lee *et al.* [53] attached folate molecules into tetrahedral DNA nanostructures for delivering siRNA into tumor cells (Figure 3.5A). Nucleic acid -based aptamers have been widely used for biosensing and diagnostic studies. Aptamers bind specifically to target molecules and have several advantages over traditional antibodies. Wide range of aptamers can be easily designed and synthesized, which allows the production of highly sensitive and specific aptamers for biosensor applications. [54] In addition, DNA origami method could provide a non-invasive way to deliver protein- and peptide-based vaccines and immunoglobulins, which are commonly injected to the patient. Vaccines and immunoglobulins could be coupled with DNA origamis via biotin-avidin interaction, DNA-protein linkage or by using aptamer-target interactions. [52] Moreover, Ora *et al.* [55] showed that enzymes attached to tubular origamis can be delivered into cells without loosing the enzymes activity. This demonstrates that DNA origamis could be used in enzyme replacement therapy or in transporting other pivotal molecules. [55] For instance, anticancer drug Doxorubicin (Dox) could be coupled into DNA nanostructures as it can bind non-covalently into double-stranded DNA (dsDNA). Uncoupled doxorubicin has poor selectivity and can cause severe side-effects. [56] Jiang *et al.* [57] showed that the cellular internalization of Dox increased when it was coupled to triangular-shaped DNA origami (Figure 3.4B). In similar study, Zhao *et al.* [58] showed that the encapsulation efficiency and drug release kinetics could be controlled by tuning the twisting of a rod-like DNA origami structure for Dox delivery. (Figure 3.5A)

DNA origami structures have been studied as carrier systems to interact with the cellular machinery on the molecular level. Schüller *et al.* [59] studied the potential of using DNA origamis as programmable and noncytotoxic immunostimulants. Hollow 30-helix DNA origami tubes (Figure 3.5C) were covered with 62 cytosine-phosphate-guanine (CpG) oligonucleotides and transfected into spleen cells of mice. Unmethylated CpGs are characteristic of microbial DNA and thus recognized by the Toll-like receptors (TLR9) of mammalian immune system as a signal for pathogen invasion. TLR9s are localized in endosomes and their activation leads to the secretion of proinflammatory cytokine mediators, which further stimulate the immune system. [59]

This kind of delivery system for intracellular signal triggering could be used in intelligent drug carriers. Moreover, since the activation of TLR9 induces both the innate and the adaptive immune system, it could be used for the immunotherapy of infectious diseases, cancers, allergies and asthma [52].

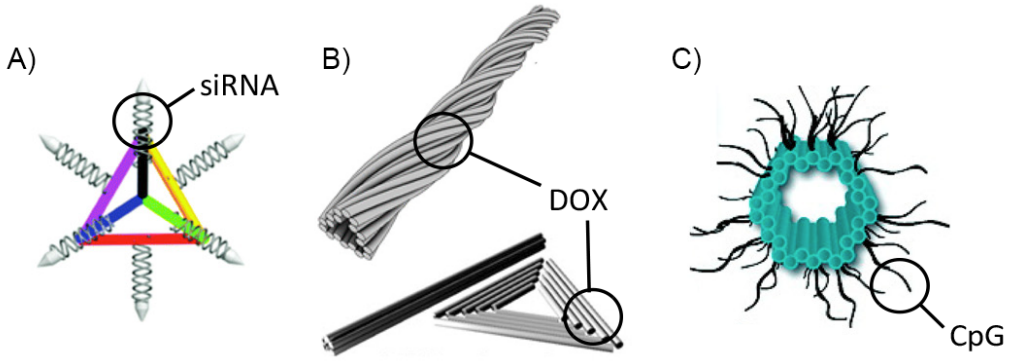

Figure 3.5: DNA-based drug-delivery carriers. A) A tetrahedral DNA nanostructure for targeted small interfering RNA (siRNA) delivery [53]. B) A rod-like [58] and a triangular-shaped [57] DNA origamis for delivering doxorubicin (DOX) for cancer cells. C) Side view of a hollow DNA origami tube for CpG-triggered immunostimulation [59]. Figure adapted from [60].

3.3.4 Functional nanomechanical molecular devices

Recently, various kinds of functional nanomechanical molecular devices have been developed using the DNA origami method. The simplest nanomechanical devices are dynamic DNA origami structures with transformation capability, such as DNA boxes with opening and closing mechanisms. Andersen *et al.* [61] were the first ones to create a DNA origami box (Figure 3.6A) from the M13 scaffold by folding six interconnecting DNA sheets. The sheets were connected at the vertices to form the box, and one of the sheets acted as a lid that could be opened and closed with a dual lock-key system. The box can be kept closed by binding the complementary DNA strands in the lid and the adjoining face, and opened by displacing the DNA strand on the lid with externally added DNA strands that bind to the sticky-end extensions in the adjoining interface.

More sophisticated nanomechanical molecular devices include DNA origami pinching devices that can be used to detect several molecules, such as metal ions and proteins [36]. Douglas *et al.* [37] created a DNA nanorobot that is capable of transporting molecular payloads to cells and sense inputs from

cell surfaces in order to activate and reconfigurate for payload delivery (Figure 3.6B). The hexagonal barrel -shaped device consists of two domains that are attached by an aptamer-encoded logic gate, and can be loaded with various cargos that can be released in a controlled way. The mechanical control of DNA origami structural changes allows DNA origamis to be used as suppressors in a transcription regulation system [62].

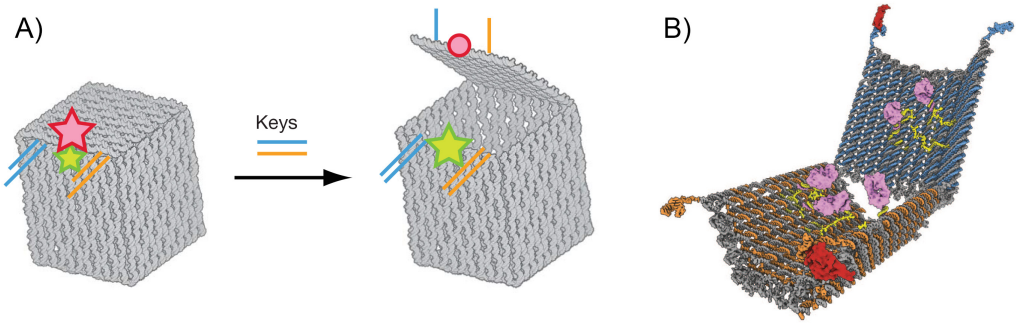

Figure 3.6: A) DNA box with a controllable lid. Adapted from [61]. B) A logic-gated DNA nanorobot capable of transporting molecular payloads and sense inputs from cells. Adapted from [37].

3.4 Biocompatibility and stability of DNA-based nanostructures

As described above, DNA nanostructures could find intriguing applications as bionanotechnological devices and drug-delivery vehicles. Therefore, questions about their biocompatibility have been raised. In general, DNA molecules are well suited for both *in vitro* and *in vivo* applications, since they are inherently non-toxic as they are naturally found in living organisms [4]. Several studies have shown that DNA nanostructures do not exhibit cytotoxicity at typical concentrations, and do not affect the viability of cells. Jiang *et al.* [57] studied triangular-shaped DNA origami structures as carriers for the circumvention of drug resistance. In their cell viability assay, no cell-toxicity was observed after 48-hour incubation with human breast adenocarcinoma cancer cells. Moreover, Zhang *et al.* [63] studied triangular DNA origamis as an *in vivo* drug delivery vehicle for cancer therapy. Nude mice were treated with the nanocarrier to study the systematic toxicity. Blood analysis after six hours did not indicate any abnormal values.

In addition to non-toxicity, the structural integrity of DNA nanostructures in biological conditions needs to be considered. Cells and organisms have complex mechanisms to detect and degrade damaged endogenous DNA and foreign DNA from invading pathogens [4]. Therefore, one of the biggest challenges for synthetic nucleotide-based construct materials is to escape and survive from this natural defense mechanism. The concentration of circulating DNA in human serum is typically rather low, between 5–40 ng/ml. However, its concentration may rise up to 1500 ng/ml during illnesses, such as autoimmune and malignant diseases. Natural helical DNA is degraded rapidly in blood serum by nuclease enzymes that cleave the phosphodiester bonds between nucleotide subunits. Moreover, antibodies, such as human immunoglobulin G (IgG) can recognize and hydrolyze B-DNA, A-DNA and Z-DNA. [64] The mean half-life for circulating DNA is usually 10–15 minutes and it is removed by the liver [65].

Topological and conformational rearrangements of DNA may reduce antibody and nuclease interactions [64]. Several *in vitro* assays have shown that small DNA nanoconstructs and DNA origami structures are more stable than double stranded plasmids of similar size. Castro *et al.* [23] showed that full digestion of honeycomb lattice structured DNA origami by deoxyribonuclease I (DNase I) endonuclease occurred ten times slower than for analogous double stranded plasmids. The tight packing in DNA origamis seems to shield from degrading enzymes. Complex set of endonucleases are also active inside cells [4], however, Mei *et al.* [66] have shown that DNA origami structures are stable in lysed cell material. The stability of DNA nanostructures in physiological conditions can be further increased by internal modifications, such as ligation, cross-linking or by using chemically modified nucleotides. Moreover, exterior protective layers, such as coating or encapsulation, could be used to shield nanostructures from endonucleases or to make them "invisible" to the immune system. [4] Perrault *et al.* [67] encapsulated DNA nanostructures with lipid bilayers to protect the origamis against nuclease digestion (Figure 3.7A). The work was inspired by viruses that have their genome and protein capsid shell in a lipid envelope. A wireframe DNA nanooctahedron was encapsulated by PEGylated lipid bilayers, which increased the structural integrity of the DNA nanostructures and also decreased the activation of the immune system.

Nucleic acids are negatively charged molecules, which makes them impermeable to the plasma membranes of cells with the same surface charge. Thus, the cellular uptake of DNA requires the use of transfection agents that can compensate the charge. By using these agents DNA nanostructures can be more readily taken up by cells. [52] Although cells uptake bare DNA origamis, low cellular uptake is one of the major challenges, along with the low stability,

in the development of DNA origami based drug delivery systems. The cellular uptake could be considerably improved with peptide-, cationic, polymer-, and intercalator-modifications [60] or by using a commercial lipid-based transfection agent Lipofectamine® [68]. Mikkilä *et al.* [69] coated rectangular shaped DNA origamis with purified cowpea chlorotic mottle virus (CCMV) capsid proteins (CP) to increase the transfection capacity (Figure 3.7B). Similarly, by coating DNA origamis with cationic polymers, the cell uptake can be increased [70]. However, other types of further improved modifications that could both enhance the cellular uptake and give protection against nucleases, are needed for sophisticated delivery systems. In this thesis, DNA origamis are coated with Janus-dendrimers and dendron-protein conjugates to improve the transfection efficiency as well as to expectedly enhance their structural integrity in biological environment.

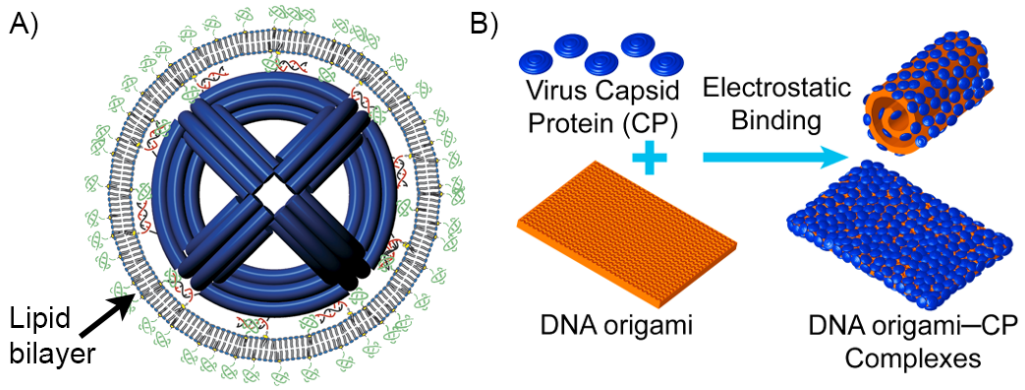

Figure 3.7: A) Virus-inspired lipid-layer encapsulation of spherical DNA origami to enhance structural integrity. Adapted from [67]. B) Self-assembly of rectangular DNA origami with virus capsid proteins (CPs) to enhance the cellular delivery of the origami. Adapted from [69].

Chapter 4

Dendrimers and multivalency

Multivalent interactions are found widely in nature and they have a key role in biological recognition events. Recently, multivalent interactions have been widely utilized in nanotechnology to assemble supramolecular materials from nanoscale objects. [71] Dendrimers are well-defined and monodisperse macromolecules, with multiple copies of a particular functionality on their surface. Thus, their unique structure enables them to engage in multivalent interactions and to be used in construction of complex structures [72]. In this thesis, dendrimers bind via multivalent and electrostatic interactions on to the surface of a DNA origami, and encapsulates the origami. This chapter first introduces dendrimers and dendrons and then discusses the central phenomena in the complexation.

4.1 Dendrimers and dendrons

Dendrimers are highly branched macromolecules with a well-defined and monodisperse structure. The first dendrimer structures were introduced in the late 1970s and early 1980s by Vögtle [73], Denkewalter [74], Tomalia [75], and Newkome [76]. Dendrimers are radially symmetrical macromolecules with symmetric branching units around a core, forming a treelike structure, as illustrated in Figure 4.1. [77] A dendron is an asymmetric half of a dendrimer. Dendrimers and dendrons have a compact molecular structure and high number of end-groups that can be functionalized in order to modify their physiochemical and biological properties [78]. Dendrimers have gained interest in a wide range of applications, particularly in supramolecular chemistry [79]. Due to many biologically relevant properties, such as polyvalency, electrostatic interactions, self-assembly, chemical stability, low cytotoxicity and solubility, dendrimers are also interesting for many biomedical applications, including

drug and gene delivery [77].

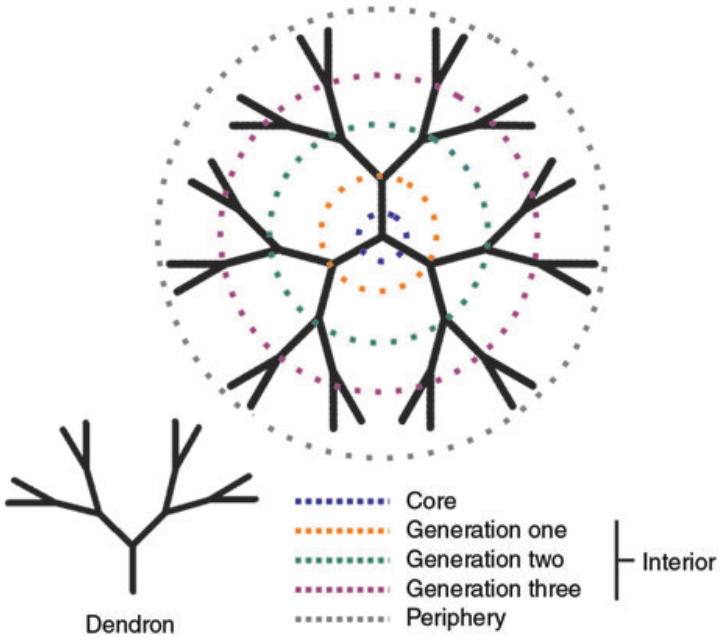

Figure 4.1: Structure of a dendrimer and a dendron. The dashed lines represent important parts of a dendrimer. [72]

Dendrimers and dendrons have three characteristic components where fascinating chemistry can occur: a central core, an interior dendritic structure and an exterior surface. By varying these components, different dendritic structures can be prepared with specific sizes and shapes. The dendrimer core is buried within the dendritic branches and thus has its own special microenvironment, which can alter the properties of chemical species attached to the core. Moreover, the shielded core is well-suited for the encapsulation of drugs and nanomaterials and thus dendrimers have great potential for applications in both biological and material sciences. The type of the core affects the cavity size, absorption capacity and capture-release characteristics of the dendrimer. From this central core, symmetric branching units grow outwards. This interior dendritic structure can accommodate several functionalities within the voids of the flexible branches. The modified environment can change the guest molecules' properties, such as solubility. [79] Moreover, a photoisomerizable dendritic core, such as an azobenzene core, allows the branches to serve as energy tunnels transferring energy to the core to induce physical and chemical changes [80]. Lastly, the multivalent dendritic surface contains a large number of functional groups that affect the dendrimer's

physiochemical and biological properties. The ability to modify the surface groups allows dendrimers to be used in applications such as sensors, light harvesting and gene delivery. [79]

Compared with synthetic polymers, which are usually polydisperse, dendrimers and dendrons are synthesized by a fully controlled step-by-step synthesis yielding nearly monodisperse structures. The ability to create monodisperse structures is extremely important to reduce experimental and therapeutical variability. There are two main synthesis strategies that are used to synthesize dendrimers and dendrons: the *divergent approach* and the *convergent approach*. In the divergent method, dendrimers and dendrons are synthesized layer-by-layer from the dendritic core, with each new layer representing a new generation of growth. New generation dendrimers and dendrons are formed by reacting the functional groups on the surface with new dendritic building blocks. This process is highly controlled, since the functional groups in the building blocks are protected until they have generated the new generation. In the convergent method, the dendrimers and dendrons are synthesized from the surface towards the core, starting with the molecular structure that will form the outermost part of the dendrimer. Thus, the final generation number of the dendrimer is pre-determined. This approach makes use of the symmetric nature of dendrimers and dendrons. [79]

Dendrimers that consist of two chemically distinct dendrons are called Janus-dendrimers. Janus-dendrimers lack the spherical symmetry that traditionally characterizes dendrimers, but can have diverse properties arising from the different dendrons. [81] Amphiphilic Janus-dendrimers consist of a hydrophilic and a hydrophobic dendron, which can self-assemble in water to form vesicles, cubosomes, disks, tubular vesicles and helical ribbons. Bilayerd vesicles called dendrosomes (Figure 4.2) mimic biological membranes and can be used in delivering drugs, proteins, genes and imaging agents. [82] Janus-dendrimers can be synthesized with three different methods. In the first method, dendrons are reacted with complementary function groups that will form the core of the Janus-dendrimer. In the second method, the first dendron is reacted with a multifunctional core, followed by a grafting of the second dendrimer to the core's other function. In the last method, the second dendron is grown into the focal point of the first dendron. [81]

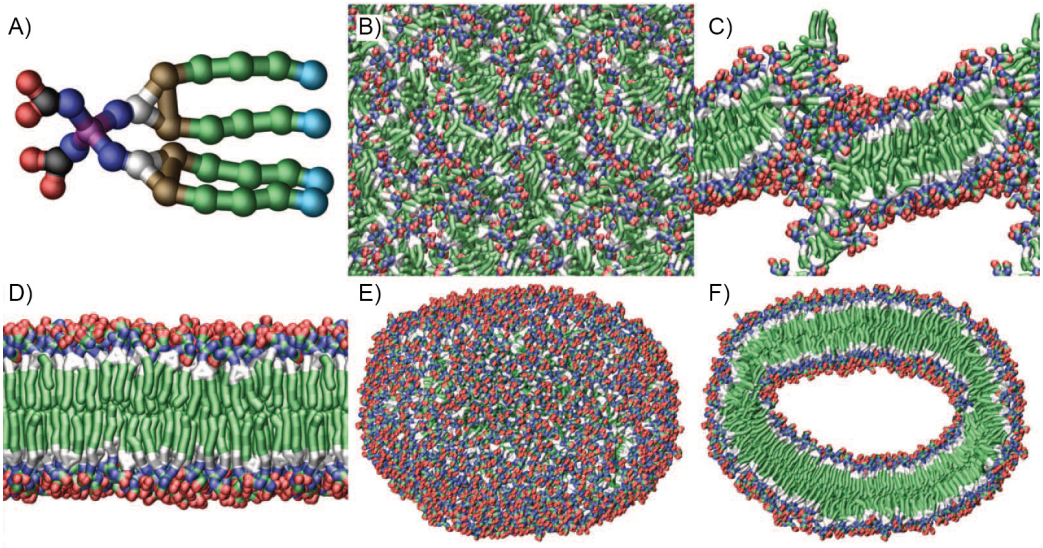

Figure 4.2: Self-assembly of Janus-dendrimers into dendrosomes. A) Model of the amphiphilic Janus-dendrimers. B) Initial snapshot before self-assembly. C) Snapshot during lamellar structure formation. D) Formed bilayer. E) Complete vesicle. F) Cross-section of the vesicle, visualizing the hollow core. [82]

4.2 Electrostatic and multivalent binding

One of the most interesting properties of dendrimers and dendrons is their multivalency – along with their well-defined structure and ease of functionalization. Electrostatic and multivalent binding play a critical role in many biological processes, such as viral infections and ligand binding to a receptor protein. The multiple copies of a particular functionality on the dendritic surface allows dendrimers and dendrons to engage in multivalent interactions that could be exploited in mimicking biological processes or in construction of complex structures. Moreover, if the end-groups are charged, dendrimers and dendrons can bind electrostatically to oppositely charged molecules and structures. For instance, polycationic dendrimers can be used to bind negatively charged DNA. [83] In this thesis, multivalent and electrostatic interactions are in a central role in the complexation of negatively charged DNA origami structures with positively charged dendrimers.

In electrostatic interactions, the distance over which the interaction is effective between charged particles in a solution, can be represented by the Debye screening length

$$\kappa^{-1} = \sqrt{\frac{\epsilon_0 \epsilon_r k_B T}{e^2 \sum_i c_i z_i^2}}, \tag{4.1}$$

where ϵ_0 is vacuum permittivity, ϵ_r is the dielectric constant of the solvent, k_B is Bolzmann coefficient, T is absolute temperature, e is elementary charge, c_i and z_i are the number densities and valencies of the electrolyte ions. Thus, the Debye screening length is affected by the change in the solute concentration: in high concentration solutes the electrostatic interactions are screened over short distances, whereas in dilute electrolytes the interactions affect over longer distances. [84] Therefore, it is important to take this into account when designing structures based on electrostatic binding, to make sure that the assembly is possible in the right electrolyte concentration for the application.

Valency means the maximum number of similar separate interactions that an entity can form with another entity. Thus, multivalency can be defined as multiple simultaneous interactions between two different entities. Multivalent interactions are non-covalent interactions, such as electrostatic interactions. They tend to be collectively much stronger than the corresponding monovalent interactions, thus enhancing the binding affinity. Multivalent binding has a central role in many biological processes, such as cell-cell communication, antibody-antigen interactions and viral infections. [85] Multivalent binding is favored in nature instead of one very strong monovalent interaction [86], most probably because adding new already existing interactions is relatively easier than evolving a new stronger one.

It should be noted that multivalency and cooperativity are two distinct phenomena. In cooperative binding, the binding of a first ligand changes the receptor's affinity to bind another ligand. Proteins that have more than one ligand binding site, usually exhibit cooperativity, like in the allosteric binding of oxygen to hemoglobin. [71] Multivalent binding can be divided into four different binding mechanisms: statistical rebinding, chelation, clustering and subsite binding, which are presented in Figure 4.3. In statistical rebinding, high concentration of ligands promotes binding, as the receptor is rapidly occupated by another ligand upon dissociation. In chelation, binding of a multivalent system decreases the dissociation rate when adjacent binding sites are bridged. An optimal spatial disposition allows multivalent assemblies to evoke the clustering of receptors, whereas in subsite binding, primary binding promotes secondary binding of another site in the same multivalent assembly. [85]

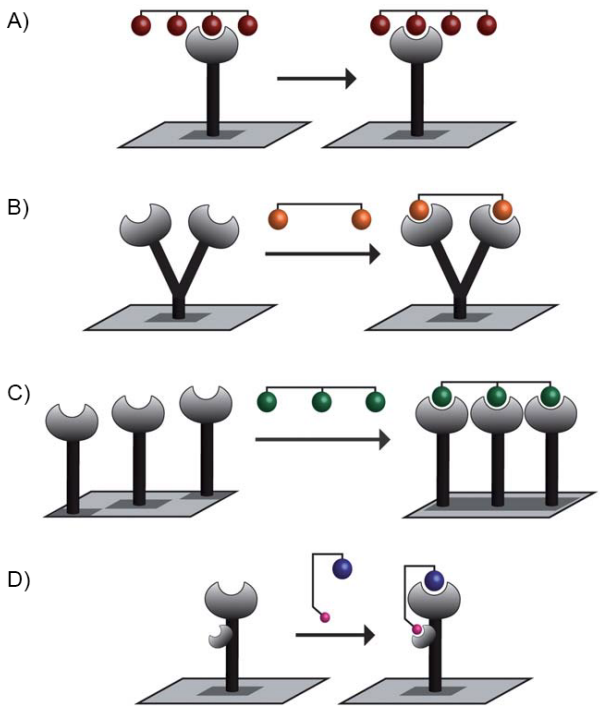

Figure 4.3: Modes of multivalent binding. A) Statistical rebinding between a receptor and a tetravalent ligand. B) Chelation between dimeric receptor and divalent ligand. C) Clustering of three receptors and a trivalent ligand. D) Subsite binding with a receptor containing a secondary binding site and a divalent ligand with two different ligand-molecules. Adapted from [85].

Chapter 5

Materials and methods

The aim of this thesis was to coat DNA origami nanostructures in order to improve the origami's structural integrity, to enhance its cellular delivery and to make the origamis invisible for the immune system. As was already discussed in Section 3.4 one of the biggest challenges with synthetic DNA nanostructures is their susceptibility to nuclease degradation and hydrolysis by antibodies in biological conditions. Moreover, the cellular delivery of DNA origamis is poor due to their polyanionic nature. Thus, in order to use DNA origamis in cellular applications, such as drug delivery vehicles, these issues need to be sorted. This thesis introduces a novel coating system which could find applications in sophisticated drug delivery systems and other nucleotide-based bionanotechnological devices.

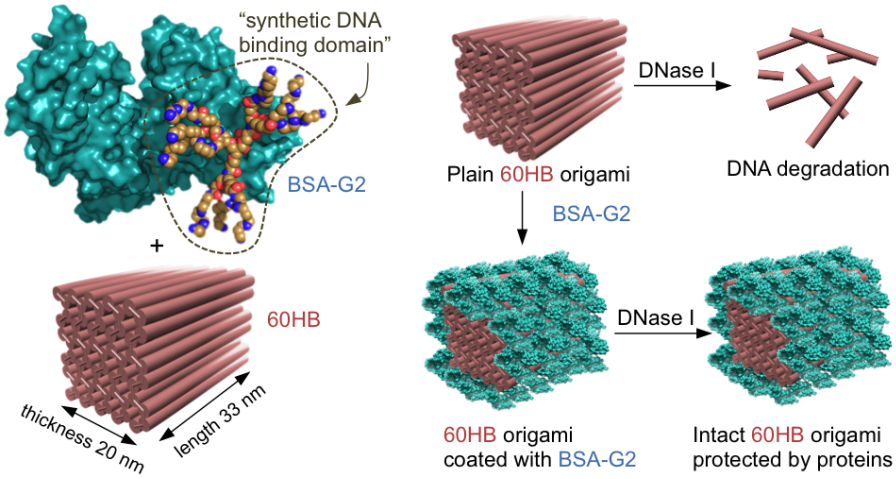

Figure 5.1: The aim of the work is to coat DNA origamis to enhance their structural integrity against nucleases and to enhance cellular delivery. [87]

5.1 Origami coatings

This work demonstrates two different coating strategies to coat DNA origamis: monolayered encapsulation of the origami with protein-dendron conjugates and a bilayered coating strategy with Janus-dendrimers. In both strategies, the binding is based on the strong electrostatic and multivalent interactions between protonated spermine tails and the polyanionic DNA origami.

5.1.1 Protein-dendron conjugates

In the monolayered encapsulation strategy, DNA origamis are coated with protein-dendron conjugates. In this work, the coating is demonstrated using two different proteins: bovine serum albumin (BSA) and hydrophobin (HFBI). Serum albumin is the most abundant protein in plasma. It is a globular protein with dimensions of 15 nm × 3.8 nm × 3.8 nm. It is synthesized in the liver and its main function is to maintain the colloid osmotic pressure of plasma. [88] As albumin is naturally occuring in plasma, it is reasoned that serum albumin coating could enhance the biocompatibility of the origami by making it invisible for the immune system. In fact, several bacteria species, such as *streptococci*, are able to bind serum albumin as they enter mammalian organisms, in order to escape from the immune system [89]. Serum albumin has been previously studied by Pitek *et al.* [90], who showed that coating of plant virus-based nanoparticles with serum albumin decreases antibody recognition. The dense coating could also form a protective layer against nuclease digestion, thus improving the circulation lifetime and the pharmacokinetic bioavailability of origamis. Moreover, serum albumin coating could enhance the cellular uptake as the coated origami is less negatively charged. In this work, bovine serum albumin (BSA) is used, which is a relatively large protein (66.4 kDa) and chemically similar to human albumin [91].

Hydrophobins are much smaller proteins (HFBI 8.7 kDa) than serum albumin, and they are expressed by filamentous fungi. Hydrophobins can be divided into two classes: class I and class II hydrophobins based on their hydropathy patterns and solubility. Hydrophobins can self-assemble at hydrophilic–hydrophobic interfaces, such as the air–water interface, into amphipathic monolayers. Hydrophobins function as adhesive proteins and they have high surface activity. [92] HFBI coating could again protect against nuclease digestion immune system activation and enhance the transfection efficiency of the origamis due to their amphiphilic structure that could form favorable interactions with cell membranes.

The proteins are chemically conjugated to polyamine dendrons that serve as the cationic binding domains that attaches to negatively charged DNA origami surface via electrostatic interaction. The dendrons contain spermine surface groups that can bind DNA with high affinity in a generation-dependent matter. Spermine is naturally found in living organism, where it binds DNA, RNA, proteins and phospholipids and is essential for cell proliferation [93]. These multivalent (either first (G1) or second (G2) -generation) Newkome-type polyamine dendrons were synthesized using the divergent methodology according to Kostiainen *et al.* [94, 95]. The proteins are attached to the dendrons via 1,4-conjugate addition of the N-maleimido group of a dendron and a free cysteine sulfhydryl group of the protein (Figure 5.2A) [95, 96]. BSA naturally contains one reactive cysteine group, whereas HFBI lacks them. Thus a free cysteine group was added to each HFBI by using site-directed mutagenesis. The protein-dendron conjugates (BSA-G1/G2 and HFBI-G1/G2) are presented in Figure 5.2B.

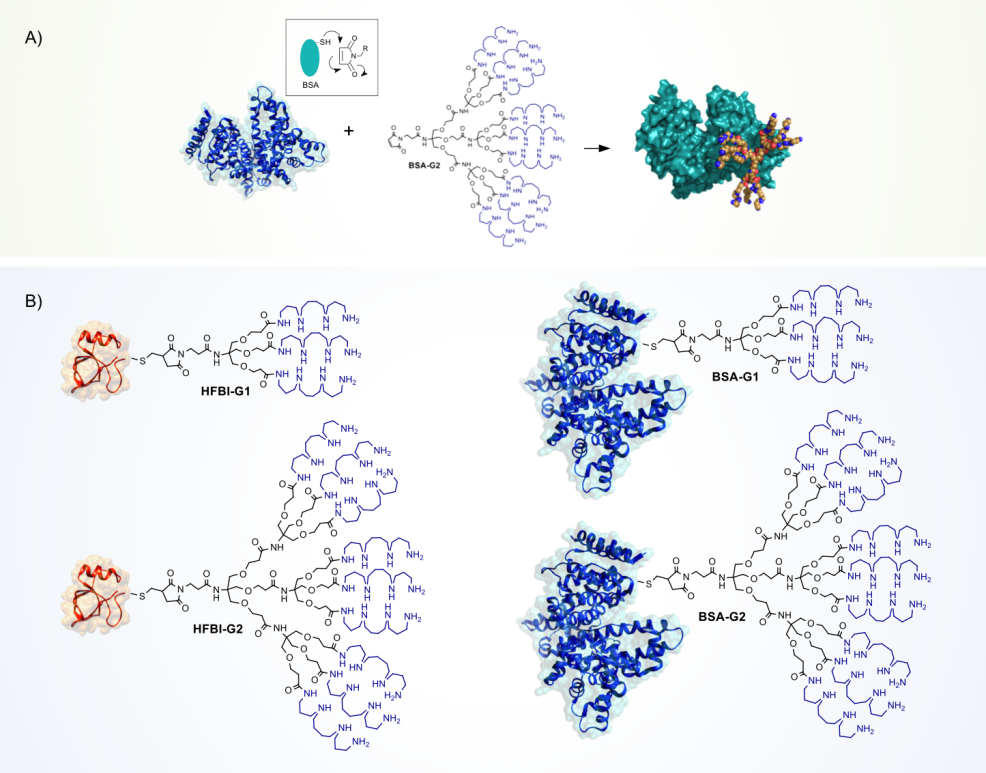

Figure 5.2: Protein-dendron conjugates used in this work. A) The proteins are linked to the polyamine dendrons via cysteine-maleimi bond. B) All used protein-dendron conjugates (HFBI-GI, HFBI-G2, BSA-G1, BSA-G2). [87]

HFBI and BSA are both known to be biocompatible, however, polycationic compounds may damage cell membranes due to the electrostatic interaction with the plasma membranes. Kostiainen [96] *et al.* studied the cytotoxicity of these protein-dendron conjugates using the methylthiazol tetrazolium (MTT) assay. The hydrophobin conjugates (HFBI-G1/G2) indicated slight cytotoxicity with high concentrations, otherwise all the proteins and their dendron conjugates were biocompatible.

5.1.2 Amphiphilic Janus-dendrimers

In the bilayerd coating strategy, DNA origamis are coated with two distinct amphiphilic Janus-dendrimers to form the protective coating over the origami. The first layer of coating is prepared with zero- or first-generation alkyl-amine dendrimers (3C12-G0 and 3C12-G1 respectively, Figure 5.3A). The dendrimers were previously synthesized by Mikkilä *et al.* [97] by combining hydrophobic Percec-type dendrons with spermine-modified Newkome-type dendron. The hypothesis is that the positively charged spermine-tails will bind to the surface of the negatively charged origami with the alkyl-tails pointing outwards.

The second layer of dendrimer-coating is formed from amphiphilic Janus-dendrimers containing alkyl-tails and polyethylene glycol (PEG) -tails (35-35-TEG, Figure 5.3B), and were previously synthesized by Nummelin *et al.* [82]. The hypothesis is, that the alkyl tails of both dendrimers will bind together due to their hydrophobicity so that eventually, the PEG tails will form the outermost layer of the bilayered coating. The PEG-coating could shield the origami from activating immune system as its known that PEG protects small therapeutical molecules against the immune system and prevents aggregation [98]. Moreover, the bilayer could efficiently protect against nuclease digestion and also enhance the transfection efficiency by making the origami less negatively charged.

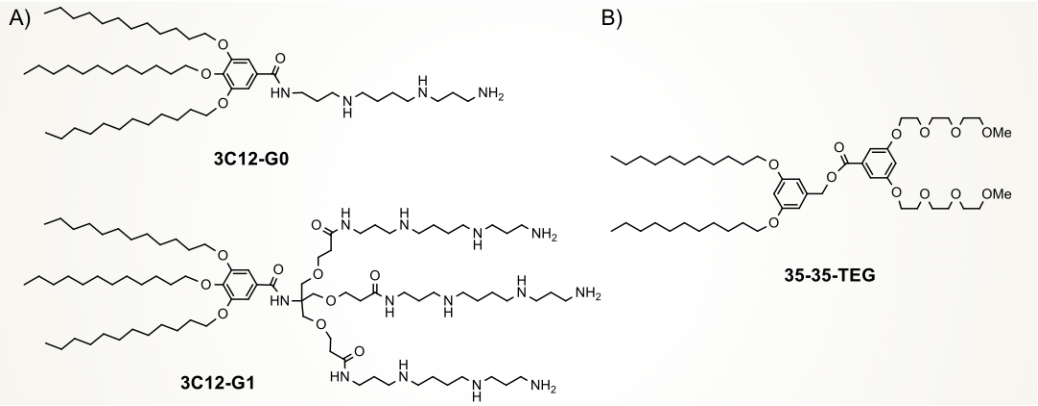

Figure 5.3: Janus-dendrimers used in this work. A) Alkyl-amine dendrimers (3C12-G0 and 3C12-G1) [97]. B) Alkyl-PEG dendrimer (35-35-TEG) [87].

5.2 Preparation of DNA origamis

A cuboid-shaped DNA origami, dubbed 60-helix bundle (60HB), was used in this work (designed by Linko *et al.* [99]). It is a cuboid-shaped structure with dimensions of approximately 20 nm × 20 nm × 33 nm. Short single stranded domains (scaffold loops) are included in the interfaces of the origami to prevent unwanted base stacking between adjacent origamis. The complete set of the staple strands for DNA origami (60HB) are listed in reference [99].

To form the designed DNA origami, the 7249 nucleotides long single-stranded scaffold strand from bacteriophage M13mp18 (Tilibit Nanosystems) was mixed with 10-fold excess of staple strands (Integrated DNA Technologies). The scaffold and staple strands were mixed with a folding buffer solution containing TAE buffer (Tris(hydroxymethyl)aminomethane, ethylenediaminetetraacetic acid (EDTA), acetic acid, pH 8.3, from Merck), magnesium chloride ($MgCl_2$) and sodium chloride (NaCl). All chemicals used in the folding, their volumes and concentrations are listed in Table 5.1

For the transfection studies, the origamis were labeled with Alexa Fluor® 488 green-fluorescent dye (Integrated DNA Technologies) to locate the origamis with confocal microscopy. Six fluorescence tags were added to one origami, three to both ends of the structure. For that, six binding sites with overhangs were added to the origami, into which the fluorescence tag modified strands could hybridize.

Final volume of 100 µl of the origami solution in a PCR tube was subjected to thermal annealing in a thermal cycler (G-storm G1 Thermal Cycler). A 58-hour annealing ramp was used: The origamis were first heated to 65 °C

Table 5.1: Folding substances

Substance	**Volume**	**Concentration**	**Final concentration**
M13mp18 (scaffold)	20 µl	100 nM	20 nM
Staple strands	40 µl	500 nM	200 nM
Folding buffer:			
TAE buffer	10 µl	10x	1x
$MgCl_2$	20 µl	100 nM	20 nM
NaCl	10 µl	50 mM	5 mM

then cooled down to 59 °C with 1.0 °C decrease in 15 minutes. From 59 °C, the solution was cooled down to 40 °C more slowly by 0.25 °C decrease in 45 minutes. Finally, the thermal cycler stored the origamis at 12 °C until the program was stopped. After folding, the origamis were stored at 4 °C.

DNA origamis were purified from excess staple strands by using PEG purification method adapted from Stahl *et al.* [28]. 200 µl of the unpurified origami solution was diluted four-fold in 1x folding buffer to obtain a starting volume of 800 µl. The solution was mixed 1:1 with PEG precipitation buffer containing 15 % PEG 8000 (w/v), 1x TAE and 505 mM NaCl. The DNA objects were then precipitated by centrifugation at 14 000 g for 30 minutes using Eppendorf Centrifuge 5424R. The pelleted materials were dissolved in 1x folding buffer at the initial volume of the starting sample. The purified samples were incubated overnight at room temperature prior to use.

5.3 Analysing DNA origamis

The quality of folding and removal of excess staple strands were analyzed with gel electrophoretic mobility shift assay (EMSA) using BIO-RAD Power Pac Basic equipment. Gel electrophoresis is a widely used method for separating DNA strands based on their size and charge. An electric field is applied to the negatively charged DNAs that move through a matrix of agarose gel. [10] 2% agarose gel was prepared by dissolving 2 g of agarose into 90 ml of 1x TAE and 10 ml of 110 mM $MgCl_2$. The solution was stained with 80 µl of ethidium bromide (EthBr) solution (0.625 mg/l). EthBr is a fluorescent tag that binds to nucleic acids and fluoresces orange color when exposed to ultraviolet light. 1x TAE with 11 mM MgCl was used as the running buffer. 10 µl of origami solution was stained with 2 µl of 6x Blue Loading Dye (New England Biolabs). 4 µl of M13mp18 scaffold diluted in 6 µl of 1x FOB and

stained with 2 µl of 6x Blue Loading Dye was used as a reference sample. 10 µl of stained samples were loaded on gel and run at constant voltage of 95 V for 45 minutes.

The DNA origami concentration was determined by UV/VIS spectroscopy. The concentration was estimated using the Beer–Lambert law,

$$A_{260} = \epsilon_{260} c_{\mathrm{DNA}} l, \tag{5.1}$$

where A_{260} is the absorbance at 260 nm wavelength, ϵ_{260} is the approximated extinction coefficient ($0.9{*}10^8$ M^{-1} cm^{-1} [100]) and l is the length of the light path in centimeters (0.05 cm). The absorbance values at 260 nm were measured with BioTek Eon microplate spectrophotometer. The calculated concentrations of the PEG-purified samples were usually between 10–15 nM.

5.4 Preparation of coated origamis

Electrostatic binding of the macromolecules to the negatively charged DNA origami was studied over a wide macromolecule/origami ratio and analyzed with EMSA. As the macromolecules bind to the origami, the electrophoretic mobility of the origami decreases as the origami's size and charge changes. Thus a shift in the electrophoretic mobility could indicate efficient coating. The electrolyte concentration in all samples was adjusted to 150 mM with NaCl to correspond to the physiological electrolyte concentration.

5.4.1 Dendron-protein coating

Purified DNA origami solution in 1x folding buffer was mixed with dendron-protein conjugate solution (BSA-G1/G2 or BSA-G1/G2), and the NaCl concentration was adjusted to 150 mM. The DNA origami concentration was 4.4 nM in all samples and the protein-dendron conjugate concentration varied from 0 to 39.3 µM to obtain the desired $c_{\mathrm{c}}/c_{\mathrm{o}}$ (conjugate concentration / origami concentration) ratio. The mixed samples were incubated 20 minutes at room temperature to allow the formation of the complexes. The samples (20 µl) were then stained with 4 µl of 6x Blue Loading Dye before loading on agarose gel to analyze the binding. The mobility of the complexes was compared with the mobility of the uncoated origami to find the optimal $c_{\mathrm{c}}/c_{\mathrm{o}}$ ratio where binding happens. In addition, transmission electron microscopy was used to verify the coating after the optimal concentration ratio was found.

5.4.2 Janus-dendrimer coating

The origamis were coated with two layers of different Janus-dendrimers to form a double layer over the origami. The dendrimers were added separately to the origami solution. Purified DNA origami solution in 1x folding buffer was first mixed with the alkyl-amine dendrimer solution (3C12-G0/G1), and the electrolyte concentration was adjusted to 150 mM with NaCl. The DNA origami concentration was 4.4 nM in all samples and the alkyl-amine dendrimer concentration varied from 0 to 157.1 µM to obtain the desired $c_{\mathrm{ad}}/c_{\mathrm{o}}$ (alkyl-amine concentration / origami concentration) ratios. The samples were incubated 15 minutes at room temperature to allow the formation of the complexes. In the preliminary studies, the samples were analyzed on gel to find the optimal $c_{\mathrm{ad}}/c_{\mathrm{o}}$ ratio before adding the second dendrimer. The samples (20 µl) were stained with 4 µl of 6x Blue Loading Dye before loading on agarose gel to analyze the binding.

After the optimal concentration for the first Janus-dendrimer was found, the second Janus-dendrimer was added to the mixture. The PEG-dendrimer (35-35-TEG) was dissolved in ethanol as it rapidly forms vesicles in water. It was dissolved in high concentration so that only a small amount of ethanol was added to the mixture as it may be toxic to cells. The final ethanol content in the samples was approximately 10 vol% and the PEG-dendrimer concentration was set to vary from 0 to 157.1 µM. The samples were incubated 15 minutes at room temperature to allow the formation of the complexes. This time the samples (22 µl) were stained with excess amount of loading dye, 5.5 µl of 6x Blue Loading Dye, to keep the samples containing ethanol, in the wells. Ethanol is less dense than water and thus the sample comes out of the well easily. The samples were loaded on gel and run at constant voltage of 95 V for 45 minutes. The mobility of the complexes was compared to the mobility of the uncoated origami.

5.5 Characterization of the coated origamis

5.5.1 Transmission electron microscopy

The samples were imaged with transmission electron microscopy (TEM) in order to verify and visualize the coating. The transmission electron micrographs were collected using JEM 3200FSC field emission microscope (JEOL) operated at 300 kV in bright field mode with Omega-type Zero-loss energy filter. The images were acquired with Gatan DigitalMicrograph software while the specimen temperature was maintained at –187 °C. The Cryo-

TEM samples were prepared by placing 3.0 µl of the aqueous dispersion on a 200-mesh copper grid with either holey carbon support film (CF-Quantifoil) or lacey carbon support film and plunge freezed in 1:1 liquid propane/ethane mixture using vitrobot with two second blotting time under 100 % humidity.

The negative staining was performed by placing 3.0 µl of the aqueous dispersion on plasma cleaned (30 seconds oxygen plasma flash) 300 square mesh copper grid with ultrathin carbon film support film. The grid with sample was then washed with droplets (30 µl) of water and three times with 3 % (w/v) of uranyl formate solution. The samples were imaged after drying under ambient conditions for 16 hours. Sample preparation without staining was performed by placing 3.0 µl of sample on a plasma cleaned 300 square mesh copper grid with carbon support film. The excess sample was removed by blotting using Whatman® No. 4 filter paper and imaged after drying under ambient conditions for 24 hours.

5.5.2 Structural integrity against nucleases

To study the structural integrity of the coated origamis, the samples were subjected to enzyme digestion by deoxyribonuclease I (DNase I) endonuclease. DNase I is primarily a secreted protein that is released into the alimentary track and blood stream. It degrades extracellular DNA released from necrotic cells or bacteria into mono- and oligonucleotide fragments by cleaving the phosphodiester linkages next to pyrimidine nucleotides. DNase I is a Ca^{2+} and Mg^{2+} dependent endonuclease. [101] In addition to being a waste-management nuclease, DNase I has been suggested to cleave DNA during apoptosis in differentiated cells [102].

The coated origamis and plain origami solution were treated with increasing amounts of DNase I (Sigma) to see whether the coating layer protects the origami. The samples were mixed into final origami concentration of 3.3 nM in 1x folding buffer and DNase I solution, so that the final volume of the sample is 20 µl and final Mg^{2+} concentration is 6 mM. The samples were treated with 0–10 U of enzyme and incubated for 1 hour at room temperature. The structure degradation was analyzed with agarose gel electrophoresis. The samples were stained with 4 µl of 6x Blue Loading Dye and loaded on 2 % agarose gel. Fading origami bands in the gel with increasing units of DNase I, indicate degradation. By calculating the relative intensities of the bands, structural integrity between uncoated and coated origamis could be compared to see whether the coating protects the origami or not.

5.5.3 Cell transfection studies

Cell transfection studies were conducted for BSA-G2 and HFBI-G2 coated origamis, and as a reference for plain origamis. The samples were transfected into human embryonic kidney 293 (HEK293) cell line. The transfection efficiency of the protein-dendron coated origamis was studied with confocal microscopy as the origamis were labeled with Alexa Fluor® 488 green-fluorescent dye tag. The transfection studies were conducted with two different origami concentrations.

HEK293 cells (10 000) were seeded on 8-well confocal chamber and attached for 24 hours. Then 100 µl of sample with 0.64 nM or 1.28 nM origami concentration was added to the cells and incubated for 12 hours. LysoTracker red (DND99, Sigma) was used to stain the lysosomes of the cells according to the manufacturer's instructions, in order to track whether the origamis will end up in lysosomes. The live cell video was taken using a confocal microscope (Leica TCS SP5) at 37 °C. In parallel, after incubating with the origamis, the cells were stained with LysoTracker red and fixed by Paraformaldehyde. Subsequently, the cell nuclei were labeled with 4',6-diamidino-2-phenylindole (DAPI) and the images were taken with confocal microscopy (Leica TCS SP5).

The transfection efficiency was quantified with fluorescence-activated cell sorting (FACS), which is a special type of flow cytometry. It separates cells based on their light scattering and fluorescent characteristics. HEK293 cells (200 000) were seeded in 24-well plate (1.0 ml/well) and attached for 24 hours. Then 1 ml of 0.32 nM origami solution was added to the cells and incubated for 12 hours. After washing with 1× Hank's Balanced Salt Solution (HBSS, pH 7.4), the cells were harvested and kept on ice. Exactly 10 000 events were collected on a LSR II flow cytometer (BD Biosciences, USA) with a laser excitation wavelength of 488 nm using FACS Diva software.

Chapter 6

Results and Discussion

This chapter presents the main results obtained with the methods introduced in the previous chapter.

6.1 Verifying the correct folding of origamis

The correct folding of the 60HB DNA origami structure was studied with agarose gel electrophoretic mobility shift assay (EMSA) and verified with transmission electron microscope (TEM). Moreover, the success of removing excess staple strands with the PEG-purification method was studied with gel electrophoresis. The EMSA results confirmed the successful folding and purification of the 60HB structure, as can be seen in Figure 6.1. The mobility of the folded origami was compared with the mobility of the scaffold. The scaffold concentration and solution conditions were the same as for the origamis. The origami band in the Figure 6.1 (middle lane) moves faster than the scaffold strand (left lane), thus indicating proper folding of the structure. The lower band for the unpurified origami (middle lane) represents the excess staple strands. They move faster in the gel than the folded origami as they are smaller in size. The band for the excess staple strands is no longer visible for the PEG-purified origami (right lane), thus indicating efficient removal of the staple strands. Cryo-TEM images also verified the correct folding of the origami, as can be seen in Figure 6.3A.

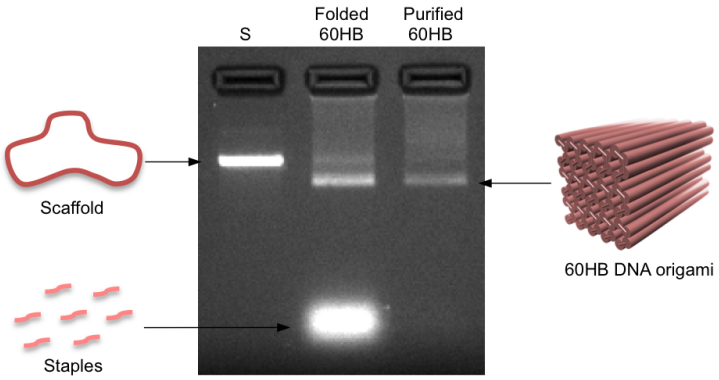

Figure 6.1: Agarose gel electrophoresis of scaffold (S) and 60HB DNA origami structure (folded and purified). The figure indicates correct folding of the 60HB as the band moves faster than the scaffold strand in the gel. It also shows efficient PEG-based purification of the 60HB from excess staple strands as the staple strand band has disappeared from the purified sample. [87]

6.2 DNA binding properties of dendron-protein conjugates

The binding of the protein-dendron conjugates on the surface of the negatively charged origami was studied with EMSA and verified with TEM. The EMSA results (Figure 6.2) indicate low binding efficiency for the first generation protein-dendron conjugates. A concentration ratio of c_c/c_o (conjugate concentration / origami concentration) = 2000 was needed for the HFBI-G1 to start immobilizing the structure. At this point, another band appeared in front of the well instead of gradually decreasing mobility of the origami band with increasing HFBI-G1 concentrations. This could indicate that the HFBI-G1 conjugates and the origamis will form large aggregates instead of individually coated origamis. BSA-G1 was not able to bind the origami as there was no shift in the electrophoretic mobility even with high concentration ratios.

The second generation protein-dendron conjugates were able to bind the 60HB DNA origami. However, the EMSA results (Figure 6.2) suggest differences in the complex formation for the HFBI and BSA-conjugates. A concentration ratio of c_c/c_o = 1000 for HFBI-G2 was needed to immobilize the structures. Another band appeared in front of the well, similarly as for the HFBI-G1 conjugates when c_c/c_o was 2000. A concentration ratio of c_c/c_o = 500 was needed for BSA-G2 to change the mobility of the origamis. In these conditions, there is a clear gradually decreasing shift in the mobility

with increasing concentration ratios. Thus, these results suggest that the BSA-G2 could efficiently coat individual origamis.

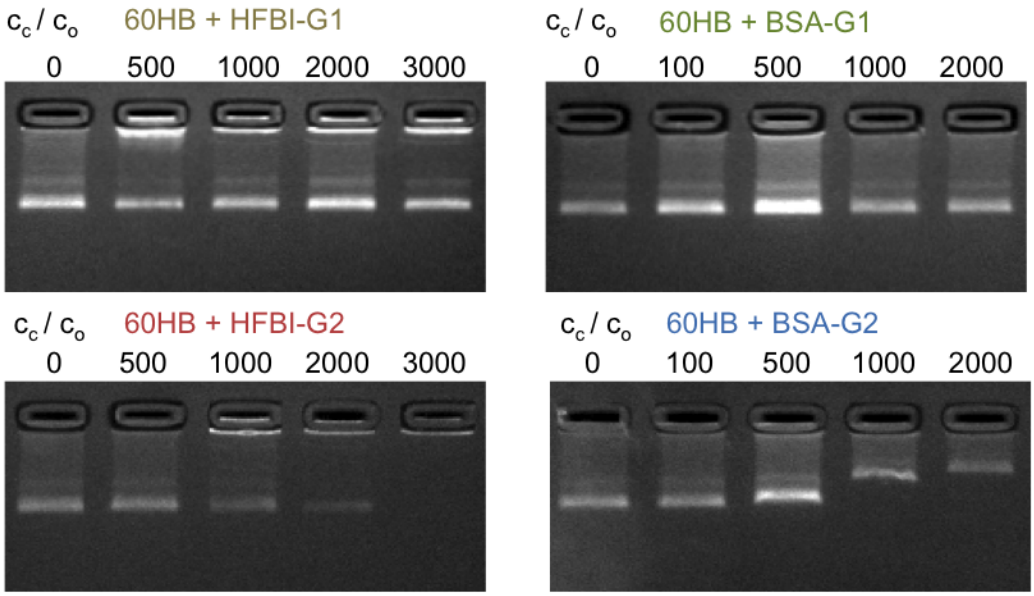

Figure 6.2: Gel electrophoretic mobility shift assay (EMSA) results for complexation of protein-dendron conjugates with 60HB. The 60HB concentration is constant (origami concentration c_o = 4.4 nM) and the HFBI-G1, HFBI-G2, BSA-G1 and BSA-G2 conjugates are added with increasing amounts (c_c/c_o = conjugate concentration / origami concentration). The EMSA results indicate low binding for the first-generation (G1) conjugates and aggregation of complexes for HFBI-G2. BSA-G2 binds efficiently as there is a clear shift in the electophoretic mobility of the samples with increasing c_c/c_o. [87]

The first generation protein-dendron conjugates did not bind as efficiently to DNA origami as the second-generation conjugates. This might be because the first generation conjugates have only three spermine tails compared with the nine spermine tails of the second-generation conjugates. As the experiments are made in physiological conditions (c(Na^+) = 150 mM), the electrolyte concentration is relatively high and the spermine tails need to compete with the counterions in the solution, and thus the electrostatic effect is screened. Therefore, more spermine tails are needed to ensure binding to DNA, and thus, multivalent second-generation conjugates can better compete with the electrolyte. In addition to the charge difference between spermine and DNA and the electrolyte concentration, also the ligand structure affects the binding. For instance, HFBI-G1 was able to bind DNA, whereas BSA-G1

was not, although they contain the same first generation dendron. BSA is a much larger protein and thus binding of the BSA-G1 conjugate is more entropically disfavored due to steric effects.

To complement the EMSA results, the binding of the HFBI-G2 (c_c/c_o = 2000) and BSA-G2 (c_c/c_o = 2000) conjugates onto the surface of the origami was verified with TEM. TEM micrographs revealed change in the size and shape of the coated origamis (Figure 6.3B) compared with the plain origamis (Figure 6.3A), indicating binding of the conjugates. Figure 6.3C shows the size distribution histograms determined from TEM micrographs for the thickness and length of the plain (red) and coated (blue) origamis. The gaussian fit shows that the dimensions of the 60HB (thickness 19.4 ± 1.8 nm, length 33.4 ± 2.1 nm) have increased approximately 12 nm with the BSA-G2 coating (thickness 31.1 ± 5.1 nm, length 45.7 ± 6.5 nm), thus indicating binding of BSA-G2 conjugates. As already deduced from the EMSA results, the TEM micrographs of HFBI-G2 coated origamis confirmed large aggregates (Figure 6.4B), which might be due to the amphiphatic nature of hydrophobins. Figure 6.4 summarizes the TEM-results.

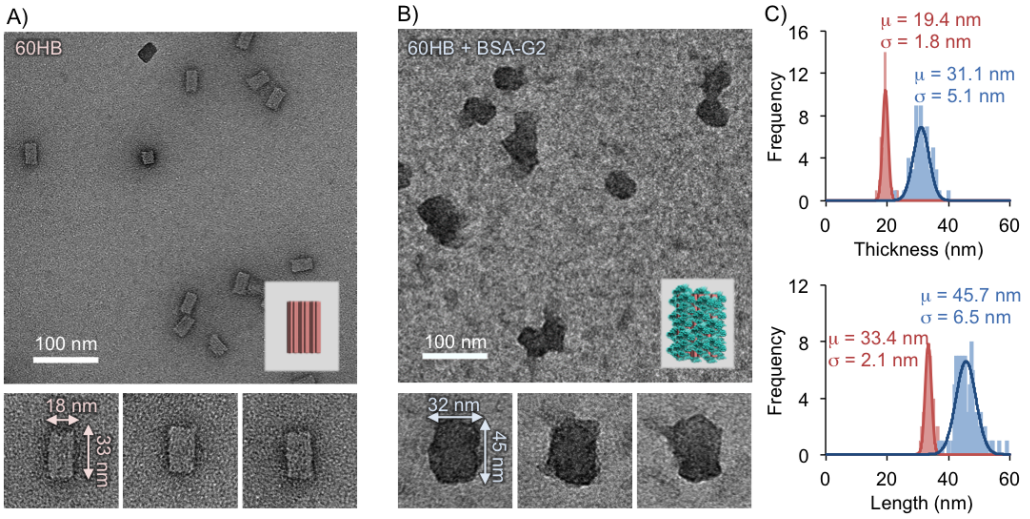

Figure 6.3: A) TEM micrograph of plain 60HB (c_o = 4.4 nM) with negative staining. B) TEM micrograph of BSA-G2 coated 60HB (c_o = 4.4 nM, c_c/c_o = 2000) indicates efficient coating as the shape and dimensions of the origami have changed. The size of the insets are 80 nm × 80 nm. C) Size distribution histograms determined from TEM micrographs. The average dimensions (μ) and standard deviation (σ) are obtained by Gaussian fitting. The thickness and length of the coated 60HB are larger than for the plain origami (red = plain origami, blue = coated origami), thus indicating efficient coating. [87]

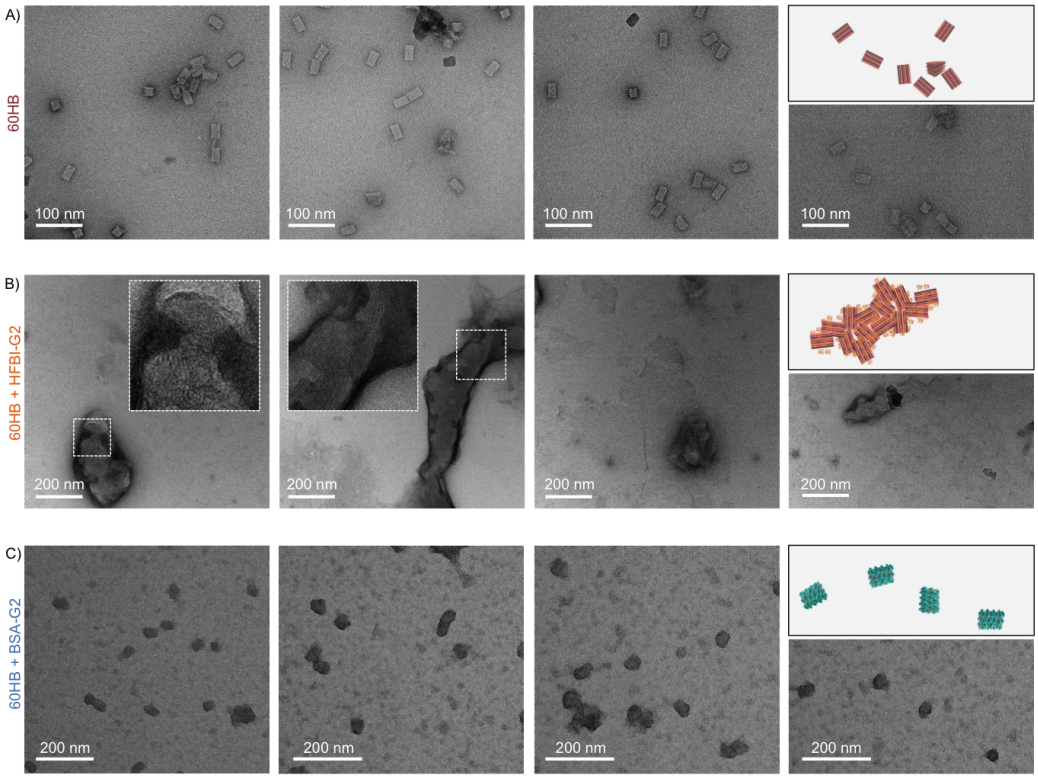

Figure 6.4: TEM micrographs of the samples. A) Plain 60HB (c_o = 4.4 nM). B) TEM-micrographs of HFBI-G2 coated origamis (c_o = 4.4 nM, c_c/c_o = 2000) revealed large aggregates. C) TEM-micrographs of individually BSA-G2 coated 60HB (c_o = 4.4 nM, c_c/c_o = 2000). [87]

6.3 DNA binding properties of the Janus-dendrimers

The binding of the Janus-dendrimers on the surface of the negatively charged origami and the formation of bilayered coating was studied with EMSA (Figure 6.5) and TEM. The origamis were first coated with increasing amounts of G0 and G1 -generation alkyl-amine dendrimers. The idea was to titrate a concentration where the dendrimers are bound on to the surface of the origami but do not yet aggregate the complexes. This way the alkyl tails should be free to bind the PEG-dendrimers that are added later. The binding of 3C12-G0 Janus-dendrimer to the origami was not strong enough even when the high concentration ratios were used (c_{ad}/c_o = alkyl-amine dendrimer concentration

/ origami concentration). However, the 3C12-G1 Janus-dendrimer was able to bind the origami: a concentration ratio of c_{ad}/c_o = 5000 was needed to start immobilizing the structure as another band appears in the gel in front of the well, thus presumably indicating aggregation. Similarly, as with the protein-dendron conjugates, the more multivalent first-generation alkyl-amine dendrimers were able to bind more efficiently than the zero-generation dendrimers, as they can better compete with the high electrolyte concentration (c(Na^+)=150 mM). In addition, as the PEG-dendrimer that should expectedly form the second layer of coating is dissolved in ethanol, the effect of ethanol in the complexation was studied before the actual addition of the PEG-dendrimer. 10 % of ethanol (v/v) was added to the samples and studied with EMSA. Ethanol did not affect the binding, as seen in Figure 6.5B.

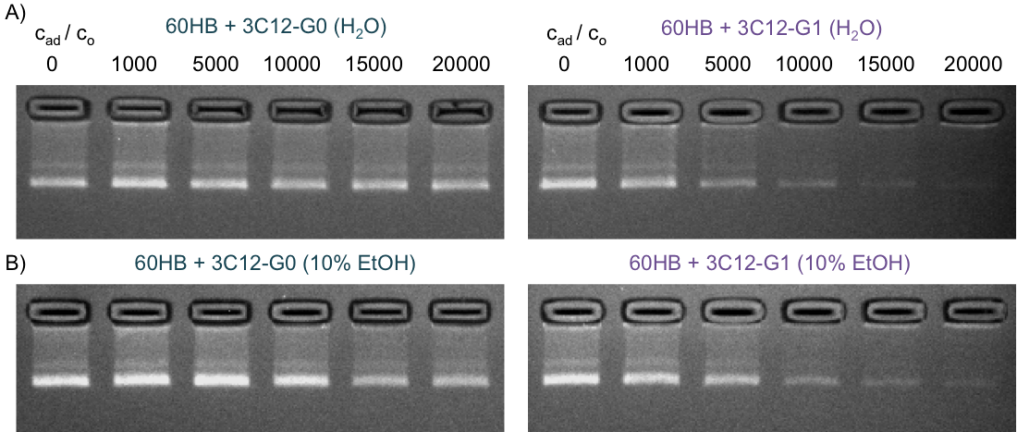

Figure 6.5: EMSA results for the alkyl-amine coating. A) 60HB concentration is constant (c_o = 4.4 nM) and the 3C12-G0 (left) and 3C12-G1 (right) -dendrimers are added with increasing amounts (c_{ad}/c_o = alkyl-amine dendrimer concentration / origami concentration). The EMSA results indicate low binding for the 3C12-G0 and aggregation of complexes for the 3C12-G1. B) Addition of EtOH did not affect the binding.

The PEG-dendrimer was added with different concentrations to the alkyl-amine coated origamis and analyzed with EMSA. First, PEG-dendrimer was added to the mixture with constant concentration (c_o = 4.4 nM, c_{pd}/c_o = 20 000) as seen in Figure 6.6. Next, samples were made with two different amine-alkyl concentrations (c_{ad}/c_o = 15 000 and 17 000), and the PEG-dendrimer concentration was changed (c_{pd}/c_o = 15 000–17 000). There was no clear sign of complexation, as all the gels looked rather similar having a band in front of the well. Consistent results were obtained when using a

concentration ratio of c_{ad}/c_{pd} =15 000:16 000, and therefore it was chosen to continue to work with. The complexes were not possible to be imaged with TEM. In addition, when considering potential applications, ethanol is problematic as it may be toxic to cells. Thus, it should be preferably removed after the complexation formation. Dialysis, spin-filtering or PEG-purification could be used to remove the ethanol.

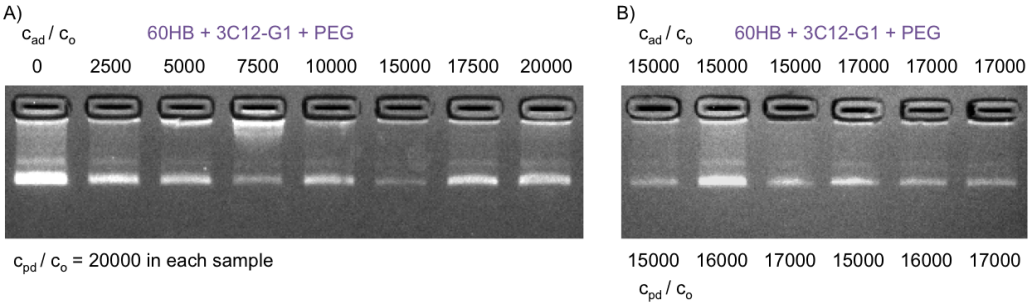

Figure 6.6: EMSA results after addition of both Janus-dendrimers. A) The origami concentration is constant (c_o = 4.4 nM) and the 3C12-G1 dendrimer is added in increasing amounts (c_{ad}/c_o = 0–20 000), while the PEG-dendrimer was added to the mixture with constant concentration (PEG-dendrimer concentration / origami concentration = c_{pd}/c_o = 20 000. B) Two different 3C12-G1 dendrimer concentrations (c_{ad}/c_o = 15 000 and 17 000) and three different PEG-dendrimer concentrations (c_{pd}/c_o = 15 000–17 000) with constant 60HB concentration (c_o = 4.4 nM) were used to analyze binding.

6.4 Determination of the structural integrity of the coated origamis

The structural integrity against nucleases digestion was studied by subjecting the coated origamis and plain origami to DNase I endonuclease. The degradation is indicated by decreasing band intensity in the gel, since the origami structure degrades and the different sized oligonucleotides move faster in the gel. To quantify the degradation, the intensity of each band was calculated from three different gels by integrating over the gel band and by normalizing the intensity of the "0 U" sample to 100 %. This way, the intensity changes of the plain origami and the coated origami could be compared. All the samples were prepared with constant 60HB concentration (c_o = 3.3 nM) and identical DNase I units (0–10 U, total volume of the samples 20 µl).

The structural integrity was studied with 60HB coated with the second-generation protein-dendron conjugates (BSA-G2 and HFBI-G2), as they showed efficient binding to the origami. As seen in Figure 6.7A, the plain 60HB DNA origami ($c_o = 3.3$ nM) degrades rapidly when subjected to DNase I digestion. This is indicated by the decreasing band intensity with increasing amount of the added DNase I. With 10 U of DNase I, the structure has almost entirely degraded as the intensity of the band is rather weak. Instead, BSA-G2 coated origamis ($c_c/c_o = 2000$) with identical DNase I units and origami concentration ($c_o = 3.3$ nM) showed enhanced structural integrity, as the band intensity did not change even with high amounts of DNase I (Figure 6.7A). Overall, the band intensity of the BSA-G2 coated origamis is lower than for the uncoated origami, as the coating most likely prevents the EthBr from binding to the origami. These results further support that the origamis are well coated with the BSA-G2 conjugates and indicate that the dense coating provides protection against nuclease digestion. The thick layer of large BSA proteins shields the origami from digestion. HFBI-G2 (c_o = 3.3 nM, $c_c/c_o = 2000$) did not protect the origamis against nucleases as the band intensity decreased indicating degradation by the nuclease.

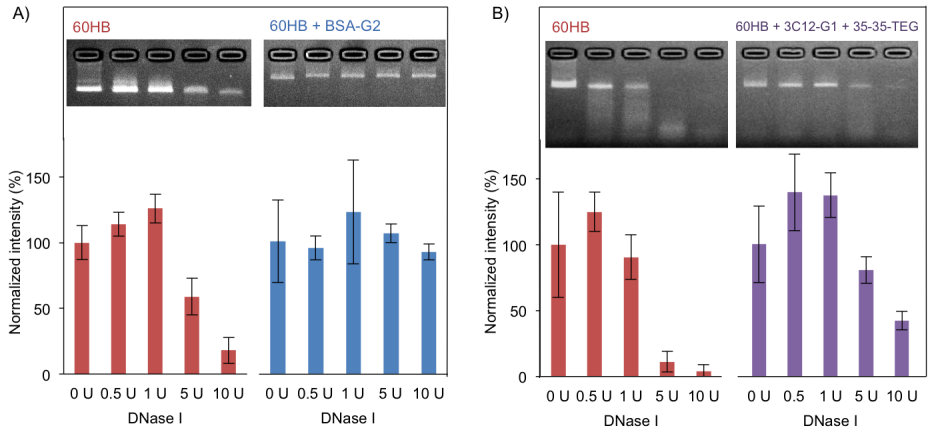

Figure 6.7: DNase I digestion results. A) Left side of the figure shows the gel electrophoresis results of the digestion for plain 60HB ($c_o = 3.3$ nM), and the normalized intensity of the bands that is calculated from three different gels. On the right side are the results for BSA-G2 coated 60HB ($c_o = 3.3$ nM, $c_c/c_o = 2000$) with identical units of DNase I. B) Similarly, left side shows digestion results for plain 60HB ($c_o = 3.3$ nM). On the right side, the 3C12-G1 + 45-35-35-TEG coated 60HB ($c_o = 3.3$ nM, $c_{ad}/c_{pd} = 15\,000{:}16\,000$) with identical units of DNAse I. Total volume of each sample is 20 µl and they were incubated for 1 hour at room temperature with the DNase I. [87]

The Janus-dendrimer coating (c_o = 3.3 nM, c_{ad}/c_{pd} = 15 000:16 000) slightly improved the structural integrity of the origamis as seen in Figure 6.7B. The results indicate at least some kind of complexation or aggregation between the macromolecules and the origami, although this was not possible to be fully proven with EMSA or TEM. The figure shows that the intensity of the Janus-dendrimer coated origami does not decrease as fast as for the plain origami with increasing units of DNase I. However, the intensity has decreased more than 50 % with 10 U of DNase I. Thus, the protection is not as efficient as for the BSA-G2 coated origamis.

6.5 Determination of the cellular delivery of the coated origamis

The transfection efficiency of the BSA-G2 and HFBI-G2 coated origamis was studied with two different origami concentrations (c_o = 0.64 nM and 1.28 nM). The first panel in Figure 6.8A shows Alexa Fluor® 488- tagged origamis after transfection (green color). The next panel represents lysosymes that have been labeled by LysoTracker (red color), and the last panel is an overlay image of the first two panels with DAPI-labeled cell nuclei. The confocal microscopy micrographs (Figure 6.8A) show that BSA-G2 (c_o = 1.28 nM, c_c/c_o = 2000) coated 60HB transfects the HEK293 cells most efficiently, as there is the highest amount of origamis visible in the figure. The plain origami (c_o = 1.28 nM) and the HFBI-G2 coated origamis (c_o = 1.28 nM, c_c/c_o = 2000) were also able to transfect cells, however, much less efficiently, as there is a lower amount of origamis visible. Figure 6.8B is an overlay image of the BSA-G2 coated origamis and lysosomes and the cells in bright field mode. It clearly shows that all the origamis do not end up in the lysosomes, which is the waste disposal system of the cells.

The quantified data of transfection obtained with FACS flow cytometry also supports the confocal microscopy results. BSA-G2 coated 60HB (c_o = 0.32 nM, c_c/c_o = 2000) transfects the HEK293 cells most efficiently, almost 2.5 times more than the bare origamis (Figure 6.8C). HFBI-G2 coated origamis (c_o = 0.32 nM, c_c/c_o = 2000) transfect only slightly better than the plain 60HB (c_o = 0.32 nM). Therefore, BSA-G2 coating provides a novel coating technique enhancing not only the structural integrity but also the transfection efficiency of the origamis.

As the origamis are individually coated with BSA, the repulsive charge between the origami and the cell membrane is compensated and the origamis enter the cell easier. While the HFBI forms only aggregates with the origami,

the particles are probably too large to be easily delivered into cells.

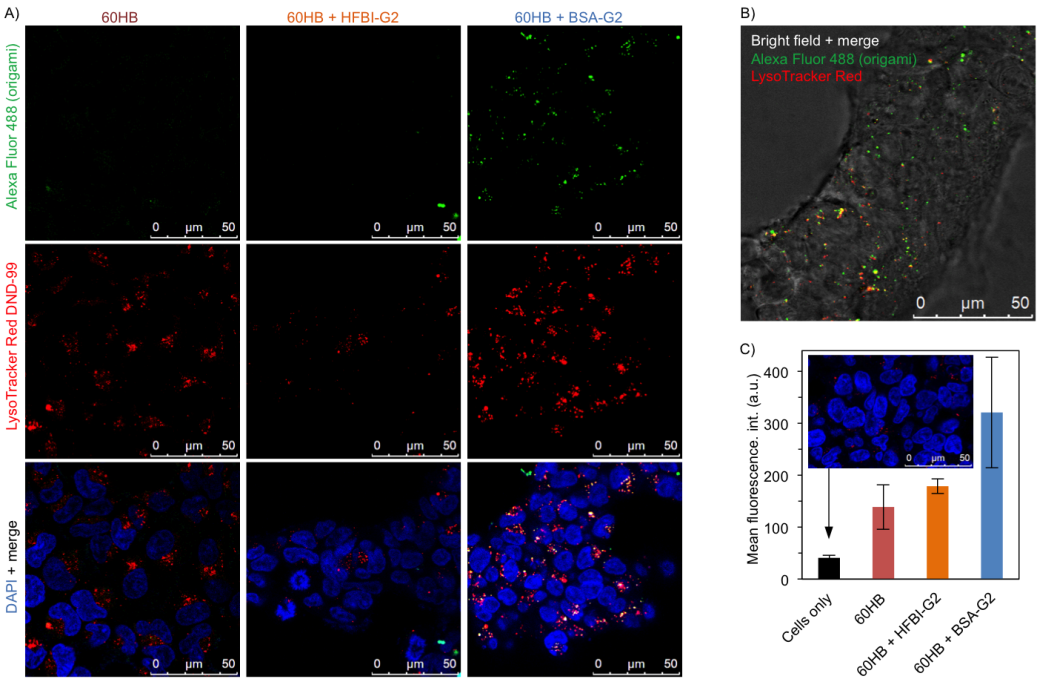

Figure 6.8: Confocal microscopy images of the transfection studies with HEK293 cell line. A) The first column represents the results for plain origami (c_o = 1.28 nM), the middle column for HFBI-G2 coated 60HB (c_o = 1.28 nM, c_c/c_o = 2000) and the last column for the BSA-G2 coated 60HB (c_o = 1.28 nM, c_c/c_o = 2000). The top panel (Alexa Fluor® 488, green) represents the origami channel, middle panel (LysoTracker, red) lysosomes and the bottom panel DAPI-labled cell nuclei and an overlay image of the top and middle panel. B) Transfection of the BSA-G2 coated origamis (c_o = 1.28 nM, c_c/c_o = 2000) (green). The image includes lysosomes (red) and the bright field image of the cells. C) Quantified data of the transfection obtained with fluorescence-activated cell sorting (c_o = 0.32 nM, c_c/c_o = 2000) shows that BSA-G2 coated origamis transfect the cells most efficiently, whereas HFBI-G2 coating enhances it only slightly. [87]

Chapter 7

Conclusions

This work demonstrated successful coating of DNA origamis with biomacromolecules to improve the structural integrity and cellular delivery of DNA origamis. Two separate coating systems were used to coat 60HB DNA origami structure both based solely on electrostatic interactions: bilayered construction strategy with two different Janus dendrimers and a single layer construction with protein-dendron conjugates. The most efficient binding in physiologically relevant salt concentrations was achieved with the second generation dendron-protein conjugates. BSA-G2 coated origamis conferred protection against nuclease digestion by DNase I. The coating also enhanced the cellular delivery of the origamis into HEK293 cell line, which was demonstrated with confocal microscopy and fluorescence-activated cell sorting.

This novel coating system could be utilized in structural DNA nanotechnology for sophisticated nucleotide-based nanoscale devices, such as DNA nanomachines, synthetic membrane channels, and programmable immunoadjuvants, as all nucleotide-based DNA nanostructures are susceptible to nuclease digestion in physiological conditions. In addition to enhancing structural integrity, this novel coating system would benefit sophisticated drug delivery or other docking devices, as it enhances the transfection efficiency of the origamis. The coating system is also highly modifiable, since the cysteine-maleimide bond between the dendron and the protein facilitates an easy attachment of other proteins with desired functionalities. Moreover, the coating could include cell-specific ligands to target the delivery for certain cells, for instance antibodies to recognize cancer cells.

The next step for developing this kind of coating system would be to study the immune activation of the coated origamis as the possible activation of the innate immune system is a major obstacle for any biomedical application of DNA nanotechnology. The hypothesis is that the protein-dendron coating would attenuate the immune response as the origamis are shielded from

immune surveillance. Moreover, the pharmacokinetic bioavailability of the coated origamis need to be further studied for drug delivery applications. It could be reasoned that the half-life time of the coated origamis would be increased, as the origamis are no longer hydrolyzed by antibodies or digested as fast by nucleases (as reported in this work). Thus, the bioavailability of the drug carriers would be increased. Lastly, the biodistribution could be studied to profile organ distribution of fluorescent tagged complexes. The coated origamis would most likely be distributed throughout the body, whereas the uncoated origamis would be removed by renal filtration, thus more of them would be located in the kidneys and bladder.

One significant challenge for the bilayered-coating strategy is the use of PEG. Although PEG is known to be anti-immunogenic, recent studies [103, 104] have shown that approximately 25 % of the population has developed anti-PEG antibodies due to extensive use of PEG in cosmetics.

Bibliography

[1] N. C. Seeman, "Nucleic acid junctions and lattices," *Journal of Theoretical Biology*, vol. 99, no. 2, pp. 237–247, 1982.

[2] V. Linko and H. Dietz, "The enabled state of DNA nanotechnology," *Current Opinion in Biotechnology*, vol. 24, no. 4, pp. 555–561, 2013.

[3] P. W. K. Rothemund, "Folding DNA to create nanoscale shapes and patterns," *Nature*, vol. 440, no. 7082, pp. 297–302, 2006.

[4] D. Smith, V. Schüller, C. Engst, J. Rädler, and T. Liedl, "Nucleic acid nanostructures for biomedical applications," *Nanomedicine*, vol. 8, no. 1, pp. 105–121, 2013.

[5] P. Alberts, B., Johnson, A., Lewis, J., Morgan, D., Raff, M., Roberts, K., Walter, *Molecular Biology of the Cell*. Garland Science, New York, 6th ed., 2015.

[6] D. Yang, M. J. Campolongo, T. N. Nhi Tran, R. C. H. Ruiz, J. S. Kahn, and D. Luo, "Novel DNA materials and their applications," *Wiley Interdisciplinary Reviews: Nanomedicine and Nanobiotechnology*, vol. 2, no. 6, pp. 648–669, 2010.

[7] D. L. Nelson and M. M. Cox, *Lehninger Principles of Biochemistry*. W.H. Freeman, New York, 4th ed., 2005.

[8] L. A. Pray, "Discovery of DNA Structure and Function: Watson and Crick," *Nature Education*, vol. 1, no. 1, pp. 1–8, 2008.

[9] D. Kuriyan, J., Konforti, B., Wemmer, *The Molecules of Life*. Garland Science, New York, 1st ed., 2012.

[10] D. M. Blackburn, G. Michael, Gait, M. J., Loakes, D., Williams, *Nucleic acids in chemistry and biology*. Royal Society of Chemistry, Oxford, 3rd ed., 2006.

[11] V. Linko, *DNA-Based Applications in Molecular Electronics*. Phd thesis, University of Jyväskylä, 2011.

[12] N. C. Seeman, "An Overview of Structural DNA Nanotechnology," *Molecular Biotechnology*, vol. 37, no. 3, pp. 246–257, 2007.

[13] R. M. Zadegan and M. L. Norton, "Structural DNA nanotechnology: From design to applications," *International Journal of Molecular Sciences*, vol. 13, no. 6, pp. 7149–7162, 2012.

[14] B. Saccà and C. M. Niemeyer, "DNA origami: The art of folding DNA," *Angewandte Chemie - International Edition*, vol. 51, no. 1, pp. 58–66, 2012.

[15] F. Zhang, J. Nangreave, Y. Liu, and H. Yan, "Structural DNA nanotechnology: State of the art and future perspective," *Journal of the American Chemical Society*, vol. 136, no. 32, pp. 11198–11211, 2014.

[16] M. Endo, Y. Yang, and H. Sugiyama, "DNA origami technology for biomaterials applications," *Biomaterials Science*, vol. 1, no. 4, pp. 347–360, 2013.

[17] A. Kuzuya and M. Komiyama, "DNA origami: Fold, stick, and beyond," *Nanoscale*, vol. 2, no. 3, pp. 310–322, 2010.

[18] E. Pound, J. R. Ashton, H. A. Becerril, and A. T. Woolley, "Polymerase chain reaction based scaffold preparation for the production of thin, branched DNA origami nanostructures of arbitrary sizes," *Nano Letters*, vol. 9, no. 12, pp. 4302–4305, 2009.

[19] R. Veneziano, S. Ratanalert, K. Zhang, F. Zhang, H. Yan, W. Chiu, and M. Bathe, "Designer nanoscale DNA assemblies programmed from the top down," *Science*, vol. 352, no. 6293, 1534, 2016.

[20] B. Högberg, T. Liedl, and W. Shih, "Folding DNA Origami from a Double-Stranded Source of Scaffold," *Journal of the American Chemical Society*, vol. 131, no. 26, pp. 9154–9155, 2009.

[21] Y. Ke, L. L. Ong, W. Sun, J. Song, M. Dong, W. M. Shih, and P. Yin, "DNA brick crystals with prescribed depths," *Nature Chemistry*, vol. 6, no. 11, pp. 994–1002, 2014.

[22] T. G. Martin and H. Dietz, "Magnesium-free self-assembly of multi-layer DNA objects," *Nature Communications*, vol. 3, p. 1103, 2012.

[23] C. E. Castro, F. Kilchherr, D.-N. Kim, E. L. Shiao, T. Wauer, P. Wortmann, M. Bathe, and H. Dietz, "A primer to scaffolded DNA origami," *Nature methods*, vol. 8, no. 3, pp. 221–229, 2011.

[24] R. Jungmann, T. Liedl, T. L. Sobey, W. Shih, and F. C. Simmel, "Isothermal assembly of DNA origami structures using denaturing agents," *Journal of the American Chemical Society*, vol. 130, no. 31, pp. 10062–10063, 2008.

[25] C. Myhrvold, M. Dai, P. A. Silver, and P. Yin, "Isothermal self-assembly of complex DNA structures under diverse and biocompatible conditions," *Nano Letters*, vol. 13, no. 9, pp. 4242–4248, 2013.

[26] C. Lin, S. D. Perrault, M. Kwak, F. Graf, and W. M. Shih, "Purification of DNA-origami nanostructures by rate-zonal centrifugation," *Nucleic Acids Research*, vol. 41, no. 2, e40, 2013.

[27] A. Shaw, E. Benson, and B. Högberg, "Purification of Functionalized DNA Origami Nanostructures," vol. 9, no. 5, pp. 4968–4975, 2015.

[28] E. Stahl, T. G. Martin, F. Praetorius, and H. Dietz, "Facile and scalable preparation of pure and dense DNA origami solutions," *Angewandte Chemie - International Edition*, vol. 53, no. 47, pp. 12735–12740, 2014.

[29] T. Liedl, B. Högberg, J. Tytell, D. E. Ingber, and W. M. Shih, "Self-assembly of three-dimensional prestressed tensegrity structures from DNA," *Nature Nanotechnology*, vol. 5, no. 7, pp. 520–524, 2010.

[30] T. Gerling, K. F. Wagenbauer, A. M. Neuner, and H. Dietz, "Dynamic DNA devices and assemblies formed by shape-complementary, non-base pairing 3D components," *Science*, vol. 347, no. 6229, pp. 1446–1452, 2015.

[31] J.-P. J. Sobczak, T. G. Martin, T. Gerling, and H. Dietz, "Rapid Folding of DNA into Nanoscale Shapes at Constant Temperature," *Science*, vol. 338, no. 6113, pp. 1458–1461, 2012.

[32] Z. Zhao, H. Yan, and Y. Liu, "A route to scale up DNA origami using DNA tiles as folding staples," *Angewandte Chemie - International Edition*, vol. 49, no. 8, pp. 1414–1417, 2010.

[33] V. Linko and M. A. Kostiainen, "Automated design of DNA origami," *Nature Biotechnology*, vol. 34, no. 8, pp. 826–827, 2016.

[34] E. Benson, A. Mohammed, J. Gardell, S. Masich, E. Czeizler, P. Orponen, and B. Högberg, "DNA rendering of polyhedral meshes at the nanoscale," *Nature*, vol. 523, no. 7561, pp. 441–444, 2015.

[35] A. Rajendran, M. Endo, and H. Sugiyama, "Single-molecule analysis using DNA origami," *Angewandte Chemie - International Edition*, vol. 51, no. 4, pp. 874–890, 2012.

[36] A. Kuzuya and Y. Ohya, "Nanomechanical molecular devices made of DNA origami," *Accounts of Chemical Research*, vol. 47, no. 6, pp. 1742–1749, 2014.

[37] S. M. Douglas, I. Bachelet, and G. M. Church, "A Logic-Gated Nanorobot for Targeted Transport of Molecular Payloads," *Science*, vol. 335, no. 6070, pp. 831–834, 2012.

[38] H. T. Maune, S.-p. Han, R. D. Barish, M. Bockrath, W. A. Goddard III, P. W. K. Rothemund, and E. Winfree, "Self-assembly of carbon nanotubes into two-dimensional geometries using DNA origami templates," *Nature Nanotechnology*, vol. 5, no. 1, pp. 61–66, 2010.

[39] A. Kuzyk, K. T. Laitinen, and P. Törmä, "DNA origami as a nanoscale template for protein assembly," *Nanotechnology*, vol. 20, no. 23, 235305, 2009.

[40] B. Ding, Z. Deng, H. Yan, S. Cabrini, and R. N. Zuckermann, "Gold Nanoparticles Self-similar Chain Structure Organized by DNA Origami," *Journal of the American Chemical Society*, vol. 132, no. 10, pp. 1–16, 2010.

[41] J. Nangreave, D. Han, Y. Liu, and H. Yan, "DNA origami: A history and current perspective," *Current Opinion in Chemical Biology*, vol. 14, no. 5, pp. 608–615, 2010.

[42] R. P. Goodman, C. M. Erben, J. Malo, W. M. Ho, M. L. Mckee, A. N. Kapanidis, and A. J. Turberfield, "A facile method for reversibly linking a recombinant protein to DNA," *ChemBioChem*, vol. 10, no. 9, pp. 1551–1557, 2009.

[43] V. Linko, M. Eerikäinen, and M. A. Kostiainen, "A modular DNA origami-based enzyme cascade nanoreactor," *Chemical Communications*, vol. 51, no. 25, pp. 5351–5354, 2015.

[44] B. Saccà, R. Meyer, M. Erkelenz, K. Kiko, A. Arndt, H. Schroeder, K. S. Rabe, and C. M. Niemeyer, "Orthogonal protein decoration of DNA origami," *Angewandte Chemie - International Edition*, vol. 49, no. 49, pp. 9378–9383, 2010.

[45] J. G. Mandell and C. F. Barbas, "Zinc Finger Tools: custom DNA-binding domains for transcription factors and nucleases," *Nucleic Acids Research*, vol. 34, pp. 516–523, 2006.

[46] S. Pal, Z. Deng, B. Ding, H. Yan, and Y. Liu, "DNA-origami-directed self-assembly of discrete silver-nanoparticle architectures," *Angewandte Chemie - International Edition*, vol. 49, no. 15, pp. 2700–2704, 2010.

[47] A. Kuzyk, R. Schreiber, Z. Fan, G. Pardatscher, E.-M. Roller, A. Högele, F. C. Simmel, A. O. Govorov, and T. Liedl, "DNA-based self-assembly of chiral plasmonic nanostructures with tailored optical response," *Nature*, vol. 483, no. 7389, pp. 311–314, 2012.

[48] Y. Ke, S. Lindsay, Y. Chang, Y. Liu, and H. Yan, "Self-assembled water-soluble nucleic acid probe tiles for label-free RNA hybridization assays," *Science*, vol. 319, no. 5860, pp. 180–183, 2008.

[49] Y. Sannohe, M. Endo, Y. Katsuda, K. Hidaka, and H. Sugiyama, "Visualization of dynamic conformational switching of the G-quadruplex in a DNA nanostructure," *Journal of the American Chemical Society*, vol. 132, no. 46, pp. 16311–16313, 2010.

[50] H. K. K. Subramanian, B. Chakraborty, R. Sha, and N. C. Seeman, "The label-free unambiguous detection and symbolic display of single nucleotide polymorphisms on DNA origami," *Nano Letters*, vol. 11, no. 2, pp. 910–913, 2011.

[51] N. V. Voigt, T. Tørring, A. Rotaru, M. F. Jacobsen, J. B. Ravnsbæk, R. Subramani, W. Mamdouh, J. Kjems, A. Mokhir, F. Besenbacher, and K. V. Gothelf, "Single-molecule chemical reactions on DNA origami," *Nature Nanotechnology*, vol. 5, no. 3, pp. 200–203, 2010.

[52] J. Li, C. Fan, H. Pei, J. Shi, and Q. Huang, "Smart drug delivery nanocarriers with self-assembled DNA nanostructures," *Advanced Materials*, vol. 25, no. 32, pp. 4386–4396, 2013.

[53] H. Lee, A. K. R. Lytton-Jean, Y. Chen, K. T. Love, A. I. Park, E. D. Karagiannis, A. Sehgal, W. Querbes, C. S. Zurenko, M. Jayaraman,

C. G. Peng, K. Charisse, A. Borodovsky, M. Manoharan, J. S. Donahoe, J. Truelove, M. Nahrendorf, R. Langer, and D. G. Anderson, "Molecularly self-assembled nucleic acid nanoparticles for targeted in vivo siRNA delivery," *Nature Nanotechnology*, vol. 7, no. 6, pp. 389–393, 2012.

[54] S. Song, L. Wang, J. Li, C. Fan, and J. Zhao, "Aptamer-based biosensors," *Trends in Analytical Chemistry*, vol. 27, no. 2, pp. 108–117, 2008.

[55] A. Ora, E. Järvihaavisto, H. Zhang, H. Auvinen, H. A. Santos, M. A. Kostiainen, and V. Linko, "Cellular delivery of enzyme-loaded DNA origami," *Chem. Commun.*, vol. 52, no. 98, pp. 14161–14164, 2016.

[56] V. Bagalkot, O. C. Farokhzad, R. Langer, and S. Jon, "An aptamer-doxorubicin physical conjugate as a novel targeted drug-delivery platform," *Angewandte Chemie - International Edition*, vol. 45, no. 48, pp. 8149–8152, 2006.

[57] Q. Jiang, C. Song, J. Nangreave, X. Liu, L. Lin, D. Qiu, Z. G. Wang, G. Zou, X. Liang, H. Yan, and B. Ding, "DNA origami as a carrier for circumvention of drug resistance," *Journal of the American Chemical Society*, vol. 134, no. 32, pp. 13396–13403, 2012.

[58] Y.-X. Zhao, A. Shaw, X. Zeng, E. Benson, A. M. Nyström, and B. Högberg, "DNA origami delivery system for cancer therapy with tunable release properties," *ACS nano*, vol. 6, no. 10, pp. 8684–8691, 2012.

[59] V. J. Schüller, S. Heidegger, N. Sandholzer, P. C. Nickels, N. A. Suhartha, S. Endres, C. Bourquin, and T. Liedl, "Cellular Immunostimulation by CpG-Sequence-Coated DNA Origami Structures," *ACS Nano*, vol. 5, no. 12, pp. 9696–9702, 2011.

[60] V. Linko, A. Ora, and M. A. Kostiainen, "DNA Nanostructures as Smart Drug-Delivery Vehicles and Molecular Devices," *Trends in Biotechnology*, vol. 33, no. 10, pp. 586–594, 2015.

[61] E. S. Andersen, M. Dong, M. M. Nielsen, K. Jahn, R. Subramani, W. Mamdouh, M. M. Golas, B. Sander, H. Stark, C. L. P. Oliveira, J. S. Pedersen, V. Birkedal, F. Besenbacher, K. V. Gothelf, and J. Kjems, "Self-assembly of a nanoscale DNA box with a controllable lid," *Nature*, vol. 459, no. 7243, pp. 73–77, 2009.

[62] M. Endo, R. Miyazaki, T. Emura, K. Hidaka, and H. Sugiyama, "Transcription regulation system mediated by mechanical operation of a DNA nanostructure," *Journal of the American Chemical Society*, vol. 134, no. 6, pp. 2852–2855, 2012.

[63] Q. Zhang, Q. Jiang, N. Li, L. Dai, Q. Liu, L. Song, J. Wang, Y. Li, and J. Tian, "DNA Origami as an In Vivo Drug Delivery Vehicle for Cancer Therapy," *ACS Nano*, vol. 8, no. 7, pp. 6633–6643, 2014.

[64] R. A. Freitas Jr., *Nanomedicine, Volume IIA: Biocompatibility*. Landes Bioscience, Texas, 1st. ed., 2003.

[65] Y. I. Elshimali, H. Khaddour, M. Sarkissyan, Y. Wu, and J. V. Vadgama, "The clinical utilization of circulating cell free DNA (CCFDNA) in blood of cancer patients," *International Journal of Molecular Sciences*, vol. 14, no. 9, pp. 18925–18958, 2013.

[66] Q. Mei, X. Wei, F. Su, Y. Liu, C. Youngbull, R. Johnson, S. Lindsay, H. Yan, and D. Meldrum, "Stability of DNA Origami Nanoarrays in Cell Lysate," *Nano Letters*, vol. 11, no. 4, pp. 1477–1482, 2011.

[67] S. D. Perrault and W. M. Shih, "Virus-inspired membrane encapsulation of DNA nanostructures to achieve in vivo stability," *ACS Nano*, vol. 8, no. 5, pp. 5132–5140, 2014.

[68] A. H. Okholm, J. S. Nielsen, M. Vinther, R. S. Sørensen, D. Schaffert, and J. Kjems, "Quantification of cellular uptake of DNA nanostructures by qPCR," *Methods*, vol. 67, no. 2, pp. 193–197, 2014.

[69] J. Mikkilä, A.-P. Eskelinen, E. H. Niemelä, V. Linko, M. J. Frilander, P. Törmä, and M. A. Kostiainen, "Virus-Encapsulated DNA Origami Nanostructures for Cellular Delivery," *Nano Letters*, vol. 14, no. 4, pp. 2196–2200, 2014.

[70] J. K. Kiviaho, V. Linko, A. Ora, T. Tiainen, E. Järvihaavisto, J. Mikkilä, H. Tenhu, N. Nonappa, and M. A. Kostiainen, "Cationic polymers for DNA origami coating – examining their binding efficiency and tuning the enzymatic reaction rates," *Nanoscale*, vol. 8, no. 22, pp. 11674–11680, 2016.

[71] J. D. Badjić, A. Nelson, S. J. Cantrill, W. B. Turnbull, and J. F. Stoddart, "Multivalency and cooperativity in supramolecular chemistry," *Accounts of Chemical Research*, vol. 38, no. 9, pp. 723–732, 2005.

[72] C. C. Lee, J. A. MacKay, J. M. J. Fréchet, and F. C. Szoka, "Designing dendrimers for biological applications," *Nature biotechnology*, vol. 23, no. 12, pp. 1517–1526, 2005.

[73] E. Buhleier, W. Wehner, and F. Vögtle, "'Cascade'-and 'nonskid-chain-like' syntheses of molecular cavity topologies," *Chemischer Informationsdienst*, vol. 9, no. 25, 1978.

[74] R. Denkewalter, J. Kolc, and W. J. Lukasavage, "Macromolecular highly branched homogeneous compound based on lysine units," U.S. Patent No. 4289872 A, 1981.

[75] D. Tomalia, H. Baker, J. Dewald, M. Hall, G. Kallos, S. Martin, J. Roeck, J. Ryder, and P. Smith, "A new class of polymers: starburst-dendritic macromolecules," *Polymer Journal*, vol. 17, no. 1, pp. 117–132, 1985.

[76] G. R. Newkome, Z. Yao, G. R. Baker, and V. K. Gupta, "Micelles. Part 1. Cascade molecules: a new approach to micelles. A [27]-arborol," *The Journal of Organic Chemistry*, vol. 50, no. 11, pp. 2003–2004, 1985.

[77] E. Abbasi, S. Aval, A. Akbarzadeh, M. Milani, H. Nasrabadi, S. Joo, Y. Hanifehpour, K. Nejati-Koshki, and R. Pashaei-Asl, "Dendrimers: synthesis, applications, and properties," *Nanoscale Research Letters*, vol. 9, no. 1, pp. 247–257, 2014.

[78] A. W. Bosman, H. M. Janssen, and E. W. Meijer, "About Dendrimers: Structure, Physical Properties, and Applications," *Chemical Reviews*, vol. 99, no. 7, pp. 1665–1688, 1999.

[79] G. M. Dykes, "Dendrimers: A review of their appeal and applications," *Journal of Chemical Technology and Biotechnology*, vol. 76, no. 9, pp. 903–918, 2001.

[80] D.-L. Jiang and T. Aida, "Photoisomerization in dendrimers by harvesting of low-energy photons," *Nature*, vol. 388, pp. 454–456, 1997.

[81] A.-M. Caminade, R. Laurent, B. Delavaux-Nicot, and J.-P. Majoral, ""Janus" dendrimers: syntheses and properties," *New Journal of Chemistry*, vol. 36, no. 2, pp. 217–226, 2012.

[82] V. Percec, D. A. Wilson, P. Leowanawat, C. J. Wilson, A. D. Hughes, M. S. Kaucher, D. A. Hammer, D. H. Levine, A. J. Kim, F. S. Bates, K. P. Davis, T. P. Lodge, M. L. Klein, R. H. DeVane, E. Aqad, B. M. Rosen, A. O. Argintaru, M. J. Sienkowska, K. Rissanen, S. Nummelin,

and J. Ropponen, "Self-Assembly of Janus Dendrimers into Uniform Dendrimersomes and Other Complex Architectures," *Science*, vol. 328, no. 5981, pp. 1009–1014, 2010.

[83] F. Zeng and S. C. Zimmerman, "Dendrimers in Supramolecular Chemistry: From Molecular Recognition to Self-Assembly," *Chemical Reviews*, vol. 97, no. 5, pp. 1681–1712, 1997.

[84] A. M. Smith, A. A. Lee, and S. Perkin, "The Electrostatic Screening Length in Concentrated Electrolytes Increases with Concentration," *Journal of Physical Chemistry Letters*, vol. 7, no. 12, pp. 2157–2163, 2016.

[85] P. M. Levine, T. P. Carberry, J. M. Holub, and K. Kirshenbaum, "Crafting precise multivalent architectures," *Medicinal Chemical Communications*, vol. 4, no. 3, pp. 493–509, 2013.

[86] M. A. Kostiainen, *Multivalent dendrons for high affinity DNA binding*. Doctoral dissertation, Helsinki University of Technology, 2008.

[87] H. Auvinen, H. Zhang, Nonappa, S. Nummelin, O. Ikkala, H. A. Santos, V. Linko, and M. A. Kostiainen, "Protein-Dendron Conjugate Coating of DNA Origami Nanostructures for Enhanced Stability and Cellular Delivery," *Submitted for publication in Nano Letters*, 2016.

[88] M. A. Rothschild, M. Oratz, and S. S. Schreiber, "Serum albumin," *Hepatology*, vol. 8, no. 2, pp. 385–401, 1988.

[89] A. Egesten, I. M. Frick, M. Mörgelin, A. I. Olin, and L. Björck, "Binding of albumin promotes bacterial survival at the epithelial surface," *Journal of Biological Chemistry*, vol. 286, no. 4, pp. 2469–2476, 2011.

[90] A. S. Pitek, S. A. Jameson, F. A. Veliz, S. Shukla, and N. F. Steinmetz, "Serum albumin 'camouflage' of plant virus based nanoparticles prevents their antibody recognition and enhances pharmacokinetics," *Biomaterials*, vol. 89, pp. 89–97, 2016.

[91] T. Peters, *All About Albumin, Biochemistry, Genetics and Medical Applications*. Academic Press, San Diego, 1996.

[92] S. Askolin, M. Linder, K. Scholtmeijer, M. Tenkanen, M. Penttilä, M. L. de Vocht, and H. A. B. Wösten, "Interaction and comparison of a class I hydrophobin from Schizophyllum commune and class II Hydrophobins Trichoderma reesei," *Biomacromolecules*, vol. 7, no. 4, pp. 1295–1301, 2006.

[93] S. Mandal, A. Mandal, H. E. Johansson, A. V. Orjalo, and M. H. Park, "Depletion of cellular polyamines, spermidine and spermine, causes a total arrest in translation and growth in mammalian cells," *Proceedings of the National Academy of Sciences of the United States of America*, vol. 110, no. 6, pp. 2169–2174, 2013.

[94] M. A. Kostiainen, J. G. Hardy, and D. K. Smith, "High-affinity multivalent DNA binding by using low-molecular-weight dendrons," *Angewandte Chemie - International Edition*, vol. 44, no. 17, pp. 2556–2559, 2005.

[95] M. A. Kostiainen, G. R. Szilvay, D. K. Smith, M. B. Linder, and O. Ikkala, "Multivalent dendrons for high-affinity adhesion of proteins to DNA," *Angewandte Chemie - International Edition*, vol. 45, no. 21, pp. 3538–3542, 2006.

[96] M. A. Kostiainen, G. R. Szilvay, J. Lehtinen, D. K. Smith, M. B. Linder, A. Urtti, and O. Ikkala, "Precisely Defined Protein–Polymer Conjugates: Construction of Synthetic DNA Binding Domains on Proteins by Using Multivalent Dendrons," *ACS Nano*, vol. 1, no. 2, pp. 103–113, 2007.

[97] J. Mikkilä, H. Rosilo, S. Nummelin, J. Seitsonen, J. Ruokolainen, and M. A. Kostiainen, "Janus-dendrimer-mediated formation of crystalline virus assemblies," *ACS Macro Letters*, vol. 2, no. 8, pp. 720–724, 2013.

[98] K. Knop, R. Hoogenboom, D. Fischer, and U. S. Schubert, "Poly(ethylene glycol) in drug delivery: Pros and cons as well as potential alternatives," *Angewandte Chemie - International Edition*, vol. 49, no. 36, pp. 6288–6308, 2010.

[99] V. Linko, B. Shen, K. Tapio, J. J. Toppari, M. A. Kostiainen, and S. Tuukkanen, "One-step large-scale deposition of salt-free DNA origami nanostructures," *Scientific Reports*, vol. 5, 15634, 2015.

[100] A. M. Hung, C. M. Micheel, L. D. Bozano, L. W. Osterbur, G. M. Wallraff, and J. N. Cha, "Large-area spatially ordered arrays of gold nanoparticles directed by lithographically confined DNA origami.," *Nature nanotechnology*, vol. 5, no. 2, pp. 121–126, 2010.

[101] K. Samejima and W. C. Earnshaw, "Trashing the genome: the role of nucleases during apoptosis," *Nature Reviews Molecular Cell Biology*, vol. 6, no. 9, pp. 677–688, 2005.

[102] Q. Y. Liu, M. Ribecco, S. Pandey, P. R. Walker, and M. Sikorska, "Apoptosis-related Functional Features of the DNaseI-like Family of Nucleases," *Annals of the New York Academy of Sciences*, vol. 887, no. 1, pp. 60–76, 1999.

[103] R. P. Garay, R. El-Gewely, J. K. Armstrong, G. Garratty, and P. Richette, "Antibodies against polyethylene glycol in healthy subjects and in patients treated with PEG-conjugated agents," *Expert Opinion on Drug Delivery*, vol. 9, no. 11, pp. 1319–1323, 2012.

[104] G. Garratty, "Modulating the red cell membrane to produce universal/stealth donor red cells suitable for transfusion," *Vox Sanguinis*, vol. 94, no. 2, pp. 87–95, 2008.